International Journal of Networks and Communications 2019, 9(1): 1-22
DOI: 10.5923/j.ijnc.20190901.01

Performance Investigation of Unamplified C-Band Nyquist 16-QAM Half-Cycle Transmission for Short-Reach Optical Communications

Mays M. Ibrahim*, Raad S. Fyath

Department of Computer Engineering, Al-Nahrain University, Baghdad, Iraq

Abstract This paper investigates the transmission performance of 16-QAM Nyquist half-cycle single-side band transmission over unamplified C-band optical fiber link. The system uses optical carrier assisted intensity modulation/direct detection scheme with digital signal processing unit is employed in the receiver to compensate fiber dispersion and nonlinear optics effect. Expressions are derived to assess the noise and bit error rate (BER) characteristics of the receiver. Results are presented to address the effect of the assisted optical carrier on the BER performance of 56, 112, 224 Gbps receivers. Simulation results are presented for 112 and 224 Gbps single-channel system to address the effect of various system parameters on the maximum reach. Then the simulation is extended to WDM system incorporating with 112 and 224 Gbps channel data rates. Simulation results obtained using Optisystem software reveal that a maximum reach of 86 and 65 km is achieved for 32×112 Gbps (≈ 3.6 Tbps) and 32×224 Gbps (≈ 7.2 Tbps) system, respectively, with 0 dBm signal and carrier lasers powers.

Keywords Nyquist half cycle optical communication, Unamplified C-band, 16-QAM IM/DD, Optical SSB 16-QAM

1. Introduction

The demand for high-capacity communication services continues to grow at around 30% to 60% per year with increase data delivery in both long-haul backbone and short-haul optical network [1-3]. This capacity demand has attracted intense research on high-spectral efficiency (SE) optical communication networks [4-8]. To increase the SE of these networks, high-order modulation formats such as quadrature-amplitude modulation (QAM) have been employed [4, 5] and supported by advanced multiplexing techniques such as orthogonal frequency-division multiplexing (OFDM) [9, 10] and Nyquist wavelength-division multiplexing (WDM) [11-13]. The operation of high-data rate long-haul and metro optical networks are mainly based on coherent receivers which require complex hardware including local laser to act as a local oscillator, balanced photodiode (PD) configuration, and analog-to-digital converters (ADCs) [14-17]. The expense of coherent receiver-based scheme can be shared by a large number of subscribers which makes this high-efficiency scheme suitable for such types of optical networks. In contrast, short-reach optical network serves fewer subscribers and hence the cost and complexity of coherent detection less justifiable here. Therefore, intensity modulation/direct detection (IM/DD) schemes have attracted increasing interest for short-range applications [18-20]. The DD system only needs one single-ended PD and one ADC for each polarization in the receivers and hence it is characterized by low cost and easy integration [14, 21].

Various modulation techniques have been used for IM/DD-based short-reach optical networks [21]. Among these techniques are multilevel pulse amplitude modulation (PAM) [22-24], OFDM [24, 25], carrierless amplitude/phase (CAP) modulation [26, 27], and QAM with subcarrier modulation (SCM) [28, 29]. In general, OFDM and CAP are more complex than SCM. OFDM uses fast Fourier transform (FFT) and inverse FFT while CAP uses orthogonal filter pairs in the transmitter and receiver [30, 31]. In contrast, SCM can be implemented with relatively low complexities by digital frequency up-conversion without electrical mixer or radio frequency (RF) sources [21]. Further, SCM shares OFDM and CAP by using the complex-valued signal to modulate the subcarrier according to QAM signaling. However, the major limitation of bit rate-transmission distance product of DD optical communication system is fiber chromatic dispersion (CD). The CD introduces spectrally selective power fading distortion due to square-law photodetiction [32]. To reduce the effect of CD,

* Corresponding author:
mays.monadel@gmail.com (Mays M. Ibrahim)
Published online at http://journal.sapub.org/ijnc

single-sideband (SSB)-SCM rather than double-sideband (DSB)-SCM has been proposed to DD optical communication systems [33-35]. To reduce the effect of CD further, digital Nyquist pulse shaping has been used to realize SCM having subcarrier frequency equals half the symbol rate (half cycle) [14, 21, 36, 37]. The Nyquist half cycle (NHC) SSB–SCM achieves the most efficient bandwidth usage while ensuring zero intersymbol interference (ISI) at the decision detection time at the receiver.

In recent years, different research groups have been worked in the analysis, performance evaluation, and demonstration of NHC-SCM. For example, Liu et al. [28] experimentally demonstrated 40 Gbps 16-QAM vestigial sideband NHC-SCM transmission over 100 km dispersion-uncompensated standard single-mode fiber (SSMF). The losses of the fiber were compensated using Er-doped optical amplifier (OA) and the results show that the proposed system out performs DD-optical OFDM. Tang et al. [21] analyzed and demonstrated the transmission of single-polarization (SP) and dual-polarization (DP) 64/128-QAM NHC-SCM over unamplified SSMF. Their results show that when 3 GHz-electrical bandwidth is used, the bit-error rate (BER) of 32.5 Gbps DP 64-QAM format after 20 km fiber transmission is under 3.8×10^{-3}, and BER of 38 Gbps DP 128-QAM format is under 2.4×10^{-2}. In 2016, Zou [14] demonstrated the transmission of 200 Gbps NSC SSB-SCM over 80 km-amplified SSMF using 16-QAM signaling and DP direct detection. In 2017, Zhu et al. [36] demonstrated 224 Gbps 16-QAM NHC SSB-SCM transmission over 160 km amplified SSMF using optical carrier-assisted (OCA) technique. In their experiment, an optical carrier is added using an additional laser at the transmitter side, which is delivered along with the signal. Their results show that OCA-SSB is analogue to heterodyne detection and requires the simplest structure of DD with one single-ended PD and one ADC. A 112 Gbps 16-QAM SSB-SCM was also demonstrated over 960 km-amplified SSMF using NHC signaling and nonlinear distortion suppression technique [34]. The design and fabrication of a silicon photonic in-phase quadrature-phase (IQ) modulator for generating Nyquist shaped SSB signals was reported by Raun et al. [35]. They demonstrated 50 Gbps 16-QAM Nyquist-shaped SSB transmission over 320 km-amplified SSMF. The use of WDM technique to enhance the transmission rate of NHC SSB-SCM system also demonstrated but to a lesser extent. For instance, Zou et al. [32] demonstrated the transmission of 8×100 Gbps 16-QAM NHC signals over 320 km-amplified SSMF. All the references mentioned in the above literature survey use 1550 nm-wavelength or C-band for transmission. For O-band operation, Zhong et al. [37] demonstrated the transmission of 608 (4×152) Gbps 16-QAM NHC-SCM over unamplified SSMF. The maximum transmission distance achieved by the experiment is 10 km for the single-channel (152 Gbps) system and 2 km for the 4-channel WDM system.

It is clear from the above survey that most of the work reported in the literature about NHC-based optical communication systems are concerned on the transmission of a single-channel over amplified SSMFs. In these cases, Er-doped OA is inserted after each span of the transmission link to compensate the fiber loss. The OA may be also inserted at the transmitter-end of the fiber to boost the optical signal power or at the receiver-end side of the fiber to yield a preamplified optical receiver. The implementation of Er-doped OA requires a pumping laser source and this will increase the cost and system complexity when short-reach applications are considered. This paper addresses the transmission performance of single-channel and multichannel NHC SSB-SCM over a C-band SSMF-link implemented without optical amplification. The OCA-Nyquist SCM system proposed in [36] is used as the basic system for investigation in this paper. The noise characteristics and sensitivity of the OCA NHC SSB-SCM receiver are addressed analytically. The system is then implemented in Optisystem software environment and used to deduce simulation results describing the transmission performance. Both SP and PD configurations are considered for single-channel transmission and extended for WDM transmission. Simulation results are presented for 16-QAM system operating with bit rates of 56, 112, and 224 Gbps per polarization per wavelength.

The rest of the paper is organized as follows. Section two presents brief description and noise modeling for a single-channel NHC-SCM system operating over unamplified 1550 nm optical link. Related design issues and calculated BER characteristics are given in Section 3. Simulation results related to single and WDM transmission are given in Section four and five, respectively. Section six summarizes the main findings of this work.

2. System under Investigation

2.1. System Description

Figure 1 shows a block diagram of a single-channel OCA-SCM optical communication system implemented using IM/DD scheme. The system is based on NHC-SSB modulation supported by M-QAM signaling. At the transmitter, the input binary data is mapped into M-QAM format. Each of the real and imaginary parts of the QAM symbol is applied a PAM generator whose output passes through a root raised-cosine (RRC) filter to ensure zero ISI at the receiver decision circuit. The filtered versions of the two PAM signals are applied to an RF quadrature modulator. This modulator is driven by an RF subcarrier to modulate the two filtered PAM signals yielding I and Q modulated components. These two components are summed to yield the quadrature modulator output which is used as an electrical modulating waveform to control the intensity of a continuous-wave (CW) laser. This is achieved by using a SSB optical intensity modulator driven by quadrature modulated electrical signal to modulate the intensity of the CW laser field passing through it. This laser is called the

signal laser to distinguish it from another laser used in the system. This SSB optical modulator is implemented here using a conventional DSB optical modulator followed by a high-order optical bandpass filter (OBPF) to select one of the two generated optical SSB.

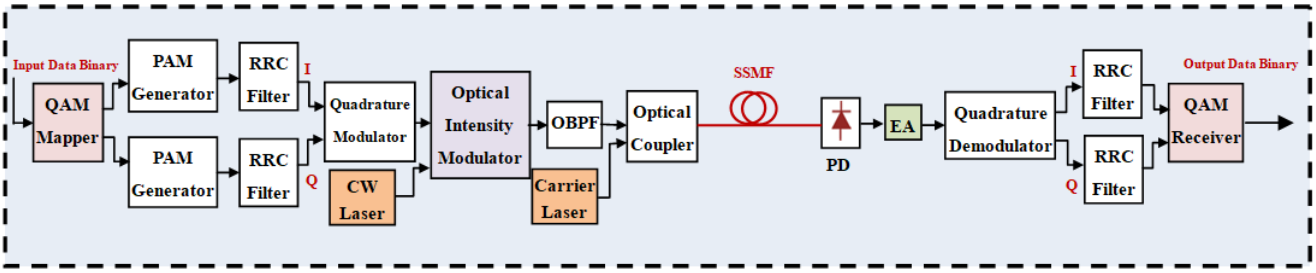

Figure 1. Block diagram of optical-carrier assisted intensity modulation/direct detection (IM/DD) system incorporating Nyquist half-cycle (NHC) single-sideband (SSB) modulation format. PAM: Pulse amplitude modulation; RRC: Root raised-cosine; CW: Continuous-wave; OBPF: Optical bandpass filter; PD: Photodiode; EA: Electronic amplifier

The modulated SSB-optical signal is then added to the output of another CW laser which acts as an assisted-carrier laser (called here the carrier laser). The combined optical waveform is lunched into a SSMF. The optical link is implemented without OAs which are usually used in conventional optical link to compensate fiber losses.

At the receiver side, the optical signal is applied to a PD which acts as an optical-to-electrical converter. The diode photogenerated current is amplified using a low-noise electronic amplifier and the resultant amplified signal is applied to an RF quadrature demodulator. The I and Q components of the demodulator output are applied to a digital signal processing (DSP) unit to compensate the effect of fiber dispersion and nonlinear optics. The I and Q components at the DSP unit output are applied to a QAM decision circuit which yields the demodulated symbols. These symbols are then converted to binary data using QAM-demaper.

2.2. System Model

Let R_b and R_s denote bit rate and QAM symbol rate, respectively. For a QAM modulation format dealing with M discrete symbol, $R_s=R_b/\log_2 M$. Let the RRC filter is designed with r roll-off factor. The DSB-bandwidth of modulated RF subcarrier is given by $2[(1+r)R_s/2]=(1+r)R_s$. When r=0, NHC shaping is achieved which has a rectangular-spectrum filter characteristic (see Fig. 2a). After optical intensity modulation, the RF signal spectrum appears as a lower sideband (LSB) and upper sideband (USB) around the signal laser frequency f_s (see Fig. 2b). A high-order OBPF of bandwidth equals $(1+r)R_s$ is used to select one of the sidebands. The LSB is choose in this work as illustrated in Fig. 2c. The field of the CW carrier laser operating with frequency $f_c=f_s+R_s/2$ is add with the LSB component of modulated optical signal to composite the transmitter optical waveform (Fig. 2.d).

The optical signal lunched at the fiber input can be expressed as

$$g(t)=[c(t)+s(t)]e_x \quad (1)$$

where c(t) is the assisted optical carrier and s(t) is the SSB optical signal. The polarization of both c(t) and s(t) are assumed to be aligned along the X-axis with e_x denotes the unit vector of the X-polarization. Further,

$$c(t)=A_c\exp(j2\pi f_c t) \quad (2a)$$

$$s(t)=A_s u(t)\exp[j2\pi(f_s-f_{sc})t] \quad (2b)$$

where

A_c = Field amplitude of the CW carrier laser.
f_c = Frequency of the CW carrier laser.
A_s = Field amplitude of the CW signal laser.
f_s = Frequency of the CW signal laser.
f_{sc} = Frequency of the RF subcarrier.
u(t) = Baseband signal with $|u(t)|\leq 1$.

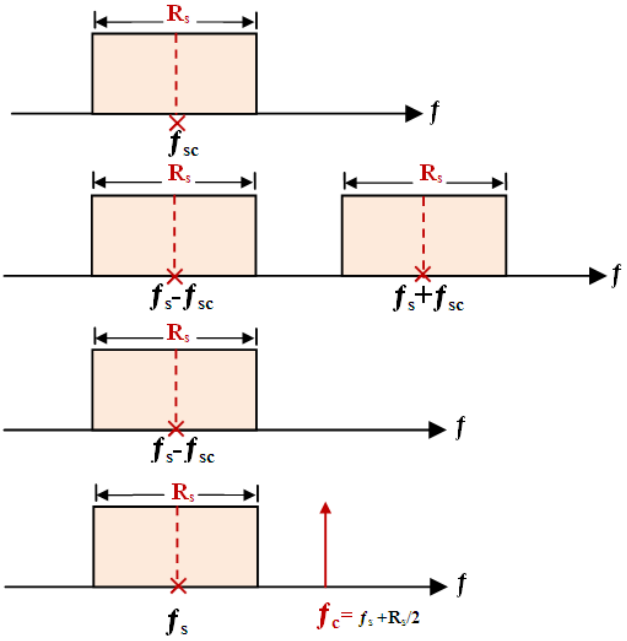

Figure 2. Illustrative spectral shapes showing the concept of NHC-SSB optical transmitter operating with OCA-technique and r=0. (a) Modulated RF subcarrier. (b) Output of the optical intensity modulator. (c) Lower SSB of the modulated optical signal. (d) Combined optical signal lunched into the fiber

Assume that the unamplified optical channel has ideal characteristics (i.e., the effect of fiber attenuation, dispersion,

and nonlinear fiber optics are negligible) and the receiver performance is dominated by the contribution of the receiver electrical noise. The receiver PD generates a photocurrent $i_{ph}(t)$ which is related to the square of the incident field amplitude

$$\begin{aligned} i_{ph}(t) &= R|c(t) + s(t)|^2 \\ &= R[|c(t)|^2+c(t)s^*(t)+c^*(t)s(t)+|s(t)|^2] \\ &= R[|c(t)|^2+2Re\{c(t)\}Re\{s(t)\}+2I_m\{c(t)\}I_m\{s(t)\}+|s(t)|^2] \\ &= R[|c(t)|^2+2Re\{c^*(t)s(t)\}+|s(t)|^2] \end{aligned} \quad (3)$$

where Re{.} And I_m{.} denote, respectively, the real and imaginary parts of the complex argument. Further, R is the PD responsitivity given by [38]

$$R = \frac{\eta q}{hf_0} \quad (4)$$

Here η is the PD quantum efficiency, q is the magnitude of electron charge, $h=6.62\times10^{-34}$ J.s is Planck's constant, and $f_0 = f_c \approx f_s$ is the frequency of the incident field.

Substituting eqns. 2a and 2b into eqn. 3 yields

$$i_{ph}(t)=RA_c^2+2RA_cA_sRe[u(t)exp\{-j2\pi(f_{If}+f_{sc})t\}]+RA_s^2|u(t)|^2 \quad (5)$$

where $f_{If} = f_c - f_s$ is the intermediate frequency (IF). According to eqn. 5, the photocurrent is splitter into three components

$$i_{ph}(t) = I_{DC} + i_s(t) + i_{s\times s}(t) \quad (6)$$

where I_{DC}, $i_s(t)$ and $i_{s\times s}(t)$ denote the direct-current (DC) component, desired signal, and signal-signal beat interference (SSBI), respectively, which are given by

$$I_{DC} = RA_c^2 \quad (7a)$$

$$i_s(t) = 2RA_cA_sRe[u(t)exp\{-j2\pi(f_{If}+f_{sc})t\}] \quad (7b)$$

$$i_{s\times s}(t)=RA_s^2|u(t)|^2 \quad (7c)$$

Few remarks concerning eqns. 7a – 7c are given here

(i) The DC component I_{DC} can be blocked by inserting a series capacitance in the current path.

(ii) The signal component $i_s(t)$ represents a DSB/suppressed carrier (SC)-modulated version of the baseband signal u(t) with an effective RF carrier having a frequency equals $(f_{If}+f_{sc})$. Coherent (synchronous) quadrature demodulator should be used to recover the signal u(t) from the component $i_s(t)$.

(iii) The SSBI component $i_{s\times s}(t)$ cannot be eliminated by any filtering process since it spectrum overlaps with the signal spectrum.

The electrical signal-to-noise ratio (SNR_e) associated with the photocurrent can be computed from

$$SNR_e = \frac{P_{se}}{P_{ne}} \quad (8)$$

where P_{se} and P_{ne} are the average powers of the signal and noise components associated with the photocurrent, respectively.

$$\begin{aligned} P_{se} &= E(|i_s(t)|^2) \\ &= 2R^2A_c^2A_s^2P_u \quad (9a) \\ &= 2R^2P_cP_s \quad (9b) \end{aligned}$$

where $P_u=E(|u(t)|^2)$. Here E(.) denotes the expectation of the argument. Further, $P_c=A_c^2$ and $P_s=A_s^2P_u$ denote, respectively, the average optical power of the assisted carrier and the signal incident on the PD.

In the absence of optical amplification, the main receiver noise components are thermal noise, which is mainly due to the front-end electronic amplifier used to amplify the photogenerated current, carrier shot noise, and signal shot noise [39]

$$P_{ne}= \sigma_{th}^2 + \sigma_{csh}^2 + \sigma_{ssh}^2 \quad (10a)$$

where σ_{th}, σ_{csh}, and σ_{ssh} denote, respectively, the standard deviations (root-mean-square (RMS)) noise currents and they are given by

$$\sigma_{th}^2 = \frac{4K_BT}{R_L}F_nB_e \quad (10b)$$

$$\sigma_{csh}^2 = 2qRA_c^2B_e = 2qRP_cB_e \quad (10c)$$

$$\sigma_{ssh}^2 = 2qRA_s^2P_uB_e = 2qRP_sB_e \quad (10d)$$

Equation 10a is well-known expression for the noise associated with electronic amplifier characterized by R_L load resistance and F_n noise figure [40]. In this equation, $K_B = 1.38\times10^{-23}$ J/k is Boltzmann constant, T is the absolute temperature (in Kelvin), and B_e is the receiver electrical bandwidth. Equations 10c and 10d are deduced from the fact that the power spectral density (PSD) of the shot noise equals (2q× average current), where q is the magnitude of the electric charge [38].

The electrical SNR of the unamplified-link system is then given by

$$(SNR_e)_u = \frac{2R^2P_c(L)P_s(L)}{\frac{4K_BT}{R_L}F_n + 2qRP_c(L) + 2qRP_s(L)} \quad (11)$$

where $P_c(L)$ and $P_s(L)$ denote, respectively, the carrier and signal power estimated at the end of the fiber link whose length is L and they are related to the power launched at the fiber input (P_{co} and P_{so}) by

$$P_c(L) = P_{co}\, e^{-\alpha L} \quad (12a)$$

$$P_s(L) = P_{so}\, e^{-\alpha L} \quad (12b)$$

Here L is the fiber length in km and α is the fiber power attenuation coefficient measured in km^{-1} and it is related to fiber loss parameter α_{dB} (measured in dB/km) by

$$\alpha_{dB} = 4.34\ \alpha \quad (13)$$

Equation 11 is then rewritten as

$$(SNR_e)_u = \frac{2e^{-\alpha L}R^2P_{co}P_{so}}{\left[\frac{4K_BTF_n}{R_L} + 2qRe^{-\alpha L}P_{co} + 2qRe^{-\alpha L}P_{so}\right]B_e} \quad (14)$$

Equation 14 is valid when the carrier laser is inserted at the

fiber input. Further, the effect of fiber dispersion on degrading the quality of the received optical signal is neglected here and this assumption is justified for dispersion-compensated or dispersion-equalized links.

For the special case when the carrier laser is inserted at the receiver side (i.e., the carrier laser field is coupled with the received signal field and the resultant waveform is applied to the PD), then eqn. 14 can be modified to cover this case

$$\left(\mathrm{SNR_e}\right)_{\mathbf{ur}} = \frac{\mathrm{e}^{-\alpha L}\mathrm{R}^2\mathrm{P_{cr}}\mathrm{P_{so}}}{\left[\frac{4\mathrm{K_B}\mathrm{TF_n}}{\mathrm{R_L}} + 2\mathrm{qRP_{cr}} + 2\mathrm{qRe}^{-\alpha L}\mathrm{P_{so}}\right]\mathrm{B_e}} \quad (15)$$

where P_{cr} is the power of the receiver-side inserted CW carrier laser. Here $(SNR_e)_{\mathbf{ur}}$ is the electrical SNR corresponding to the case of an unamplified link supported with carrier laser inserted at the receiver side.

The BER of the M-QAM demodulator used in the optical receiver is related to the electrical SNR by [36]

$$\mathrm{BER_M} = 1 - \left[1 - \frac{1}{\log_2 \mathrm{M}}\left(1 - \frac{1}{\mathrm{M}^{1/2}}\right)\mathrm{erfc}.\left(\frac{3\times\mathrm{SNR_e}}{2\left(\mathrm{M}-1\right)}\right)^{1/2}\right]^2 \quad (16)$$

where erfc(.) denotes the complementary error function

$$\mathrm{erfc}\left(\mathrm{x}\right) = \frac{2}{\left(\pi\right)^{1/2}}\int_0^{\infty}\mathrm{e}^{2\mathrm{x}}\,\mathrm{dx} \quad (17)$$

For 16-QAM signalling, eqn. 16 reduce to

$$\mathrm{BER_{16}} = 1 - [1 - 0.1875\ \mathrm{er}fc(0.1\ \mathrm{SNR_e})^{1/2}]^2 \quad (18)$$

2.3. Remarks

Few remarks are given here corresponding to the case when the unamplified link is supported by carrier laser inserted at the transmitter side. These remarks are based on eqns. 14 and 16.

(i) For a given carrier power P_c the received signal power required to achieve a certain BER level is given by

$$\mathrm{P_s}\left(\mathrm{L}\right) = \frac{\left[\frac{4\mathrm{K_B}\mathrm{TF_n}}{\mathrm{R_L}} + 2\mathrm{qRP_c}\left(\mathrm{L}\right)\right]\mathrm{B_e}\mathrm{SNR_e}}{2\mathrm{R}^2\mathrm{P_c}\left(\mathrm{L}\right) - 2\mathrm{qRB_e}\mathrm{SNR_e}} \quad (19a)$$

The SNR_e is related to the required BER by

$$\mathrm{SNR_e} = \frac{2\left(\mathrm{M}-1\right)}{3}\left[\mathrm{erfc}^{-1}\frac{\left(\mathrm{M}\right)^{1/2}}{\left(\mathrm{M}\right)^{1/2}-1}\left(1-\mathrm{BER}\right)^{1/2}\right)\right]^2 \quad (19b)$$

(ii) Consider the special case when $P_c(L) >> P_s(L)$
In this case eqn. 19a reduces to

$$\mathrm{P_s}\left(\mathrm{L}\right) \cong \left(\frac{\mathrm{S_{th}}}{2\mathrm{R}^2\mathrm{P_c}} + \frac{\mathrm{q}}{\mathrm{R}}\right)\mathrm{B_e}\mathrm{SNR_e} \quad (20)$$

where S_{th} is the power spectral density (PSD) of the thermal noise which equals σ_{th}^2/B_e. Equation 20 can be rewritten for two limiting cases corresponding to whether the thermal noise contribution σ_{th}^2 is much greater or much less than carrier shot noise contribution σ_{csh}^2

$$\mathrm{P_s}\left(\mathrm{L}\right) \cong \frac{\sigma_{\mathrm{th}}{}^2\mathrm{SNR_e}}{2\mathrm{R}^2\mathrm{P_c}\left(\mathrm{L}\right)} \quad \text{when } \sigma_{\mathrm{th}}{}^2 >> \sigma_{\mathrm{csh}}{}^2 \quad (21a)$$

In decibel measure

$$\mathrm{P_s}\left(\mathrm{L}\right)_{\mathrm{dBm}} \cong 10\log\frac{\sigma_{\mathrm{th}}{}^2}{2\mathrm{R}^2} + \mathrm{SNR_e}\left(\mathrm{dB}\right) - \mathrm{P_c}\left(\mathrm{L}\right)_{\mathrm{dBm}}$$

Note that for a given BER (i.e., given SNR_e) increasing $P_c(L)_{dBm}$ by a certain amount (i.e., Δ(dBm)) will reduce the required value of P_s (in dBm) by the same amount (i.e., Δ(dBm)).

$$\mathrm{P_s}\left(\mathrm{L}\right) \cong \frac{2\mathrm{B_e}\mathrm{SNR_e}}{\mathrm{R}} \quad \text{when } \sigma_{\mathrm{th}}{}^2 << \sigma_{\mathrm{csh}}{}^2 \quad (21b)$$

Here the received signal optical power $P_s(L)$ required to achieve a certain BER level becomes independent of $P_c(L)$.

(iii) The value of $P_c(L)$ which makes $\sigma_{th}^2 = \sigma_{csh}^2$ can be computed from

$$\mathrm{P_c}\left(\mathrm{L}\right)_{\mathrm{cross}} = \frac{2\mathrm{K_B}\mathrm{T}\,\mathrm{F_n}}{\mathrm{qRR_L}}$$

(iv) The value of $P_c(L)_{dBm}$ required to achieve a certain BER level increases linearly with $\log B_e$ when the modulated format is fixed. Therefore, the required $P_s(L)_{dBm}$ increases by 3 dBm when the bit rate doubles.

3. BER Characteristics

3.1. Design Issues

Ideally, the RF quadrature modulator in the transmitter side should use a rectangular-shape RRC filter having a bandwidth $B_{RRCF}=R_s/2$ (i.e., r=0) and RF subcarrier of frequency $f_{sc}=R_s/2$. For practical implementation, a small value of the roll-off factor r is used such as r = 0.02 to ensure that the spectrum of the output waveform of the RRC filter does not have completely Sharpe transition. This is useful to select efficiently one of the SSB components later. In this case,

$$f_{sc}=\mathrm{B_{RRCF}} = 0.5\ \mathrm{B_{RF}} = 0.5(1+\mathrm{r})\ \mathrm{R_s}$$

Note that the bandwidth of the modulated RF carrier $B_{RF}=2B_{RRCF}$ since it carries both the upper and lower SSBs (see Fig. 2). The optical modulator shifts the RF spectrum to the optical-frequency domain. The modulated optical carrier has a DSB/SC spectrum with lower and upper sidebands, each carries a copy of the RF signal spectrum. A residual optical carrier at the optical frequency f_s may exist if the optical modulator is not well-designed for DSB/SC operation and this residual carrier can be rejected by the high-order optical SSB filter.

The spectrum of the lower optical SSB extends from a low frequency $f_L = f_s - 2[0.5(1+r)R_s] = f_s - (1+r)R_s$ to a high frequency $f_h = f_s$. The OBPF used to select this sideband is

characterized by a center frequency $f_{OBPF} = (f_L+f_h)/2 = f_s\text{-}0.5(1+r)R_s$ and bandwidth $B_{OBPF}= (1+r)R_s$. The OCA laser frequency is set to $f_s+0.51R_s$.

For example, consider a 1553.5 nm (193.1 THz) 16-QAM NHC system operating with 224 Gbps bit rate. The symbol rate $R_s= R_b/\log_2 16 = R_b/4=56$ GSps. For r=0.02, $f_{sc}= (1+r)R_s$ =28.56 Gbps.

The bandwidth of the modulated RF carrier $B_{RF}=2\times28.56$ GHz=57.12 GHz. The bandwidth and center frequency of the optical SSB filter are, respectively, 57.12 GHz and $f_{OBPF} = f_s\text{-}0.5(1+r)R_s=193.1\text{-}28.56\times10^{-3}$=193.07144 THz. The filter center wavelength $\lambda_{OBPF} =c/f_{OBPF}$ =1553.829 nm.

3.2. Calculated BER Characteristics

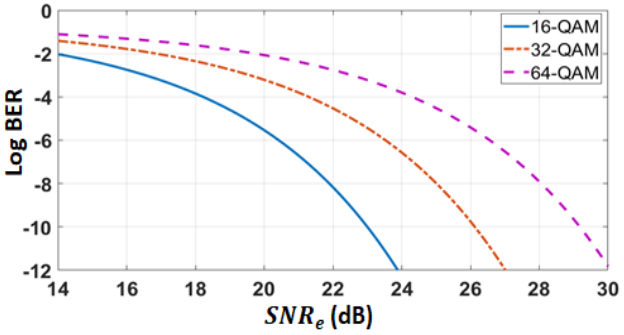

Figure 3. Variation of BER with received electrical SNR for M-QAM system

In this subsection, the BER characteristics of M-QAM NHC-SCM receiver is presented for different values of received signal power P_{sr}, received carrier power P_{cr}, number of discrete levels M (16, 32, and 64), and bit rate (56, 112 and 224 Gbps). Figure 3 illustrates the variation of BER with electrical SNR and calculated using eqn. 18 for different values of M. Note that at a fixed value of SNR_e, the results are independent of bit rate, P_{sr}, and P_{cr} since these three parameters determine the level of SNR_e used in this equation. Table 1 is deduced from Fig. 3 and shows the values SNR_e required to achieve BER=10^{-4}, 10^{-6}, 10^{-8}, and 10^{-10} for the three values of M.

Table 1. Electrical SNR required to achieve a given BER level for M-QAM receiver

BER	Required Electrical SNR (dB)		
	M=16	M=32	M=64
10^{-4}	18.3	21.3	24.4
10^{-6}	20.5	23.6	26.6
10^{-8}	21.9	25.1	28.1
10^{-10}	23.0	26.2	29.2

Figure 4 shows the dependence of BER on the received signal power P_{sr} for the 56 Gbps system and taking the received carrier power P_{cr} as an independent parameter. The calculations are repeated for 112 and 224 Gbps systems and the results are plotted in Figs. 5 and 6, respectively. From Figs. 4-6, one can deduce the receiver sensitivity, which is the minimum value of received signal power P_{sr} that gives a specific BER, as a function of carrier power at the receiver side P_{cr} and bit rate. The results are listed in Tables 2a and 2b for BER level of 10^{-10} and 4.5×10^{-3}. The last BER level corresponds to the BER limit of 7% overhead hard-decision (HD) forward-error correcting (FEC) code usually adopted in the simulation of optical networks and optical communication systems. Investigation the results in Table 2 reveals the following findings

(i) Doubling the bit rate of a given signalling format increases the receiver sensitivity by about 3 dBm.
(ii) For giving bit rate, going from 16-QAM to 32-QAM increases the receiver sensitivity by about 2.4 dBm. This is to be compared with about 2.3 dBm when one goes from 32-QAM to 64-QAM signalling.

Table 2. Sensitivity of SSB NHC receiver as a function of bit rate and modulation order when the carrier power at the receiver side equals

(a) 10 µw.

System Modulation Format	Receiver Sensitivity (dBm)					
	BER = 10^{-10}			BER = 4.5×10^{-3}		
	56 Gbps	112 Gbps	224 Gbps	56 Gbps	112 Gbps	224 Gbps
16-QAM	-28.96	-25.95	-22.94	-36.56	-33.55	-30.54
32-QAM	-26.55	-23.72	-20.81	-34.14	-31.32	-28.40
64-QAM	-24.24	-21.45	-18.44	-32.08	-29.29	-26.28

(b) 100 µw.

System Modulation Format	Receiver Sensitivity (dBm)					
	BER = 10^{-10}			BER = 4.5×10^{-3}		
	56 Gbps	112 Gbps	112 Gbps	56 Gbps	112 Gbps	224 Gbps
16-QAM	-34.84	-31.83	-28.82	-42.44	-39.43	-36.42
32-QAM	-32.43	-29.60	-26.69	-40.02	-37.20	-34.28
64-QAM	-30.12	-27.33	-24.32	-37.96	-35.17	-32.16

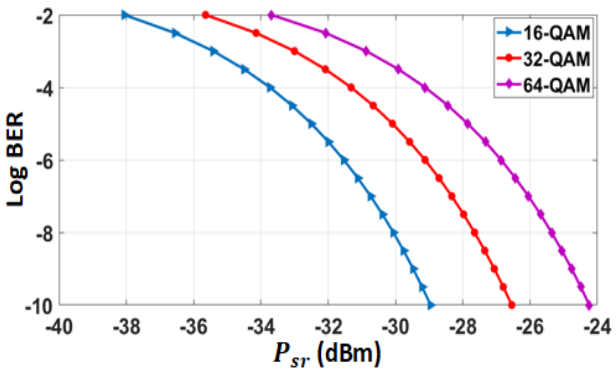

(a)

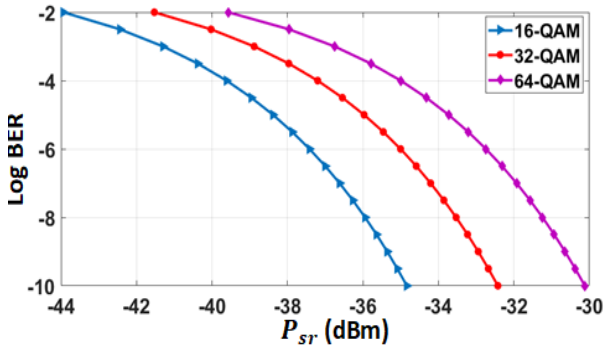

(b)

Figure 4. Dependence of BER on received signal power for 56 Gbps system. (a) P_{cr}=10 µw. (b) P_{cr}=100 µw

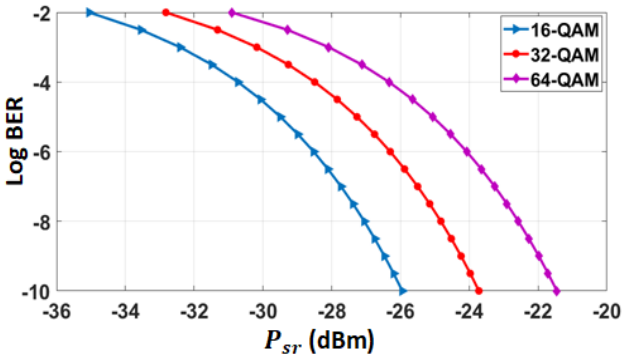

(a)

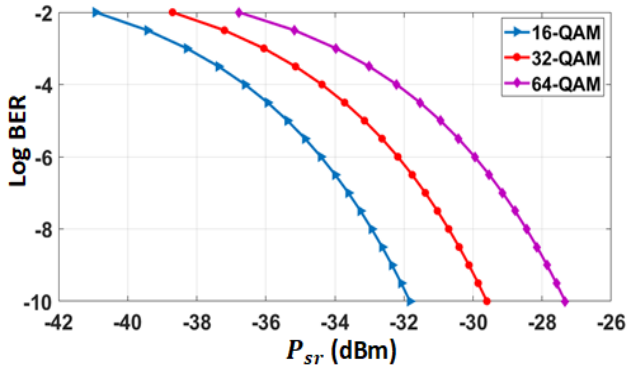

(b)

Figure 5. Dependence of BER on received signal power for 112 Gbps system. (a) P_{cr}=10 µw. (b) P_{cr}=100 µw

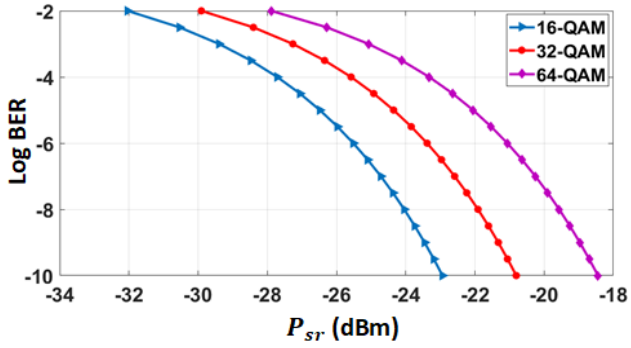

(a)

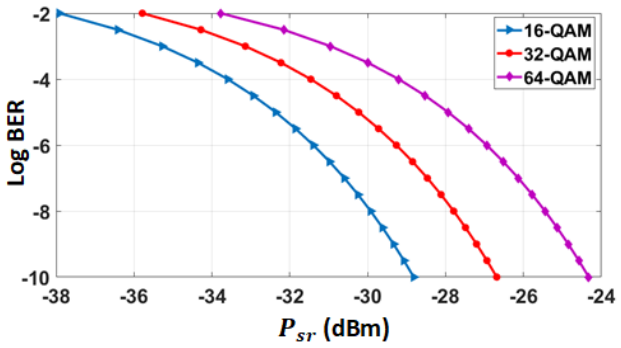

(b)

Figure 6. Dependence of BER on received signal power for 224 Gbps system. (a) P_{cr}=10 µw. (b) P_{cr}=100 µw

Figures 7a-c illustrate the receiver P_{cr}-P_{sr} characteristics at BER =4.5×10^{-3} for 56, 112, and 224 Gbps data rates, respectively. Each figure contains three plots corresponding to 16-, 32-, and 64-QAM modulation format, respectively, when the carrier laser is inserted at the transmitter side. Note that at R_b=56 Gbps, the required values of P_{sr} are -36.56, -34.14, and -32.08 dBm for 16-, 32-, and 64-QAM signalling, respectively, when P_{cr}= -20 dBm. Increasing P_{cr} to -8 dBm reduces the required values of P_{sr} to -42.98, -40.57, and -38.50 dBm, respectively. For R_b=112 Gbps P_{sr}= -33.55, -31.32, and -29.29 dBm when P_{cr}= -20 dBm and -39.97, -37.74, and -35.71 dBm when P_{cr}= -8 dBm. These values are to be compared with P_{sr}= -30.54, -28.40, and -26.28 dBm when P_{cr}= -20 dBm and -36.96, -34.83, and -32.70 dBm when P_{cr}= -8 dBm for 224 Gbps. These results are illustrated graphically in Fig. 8.

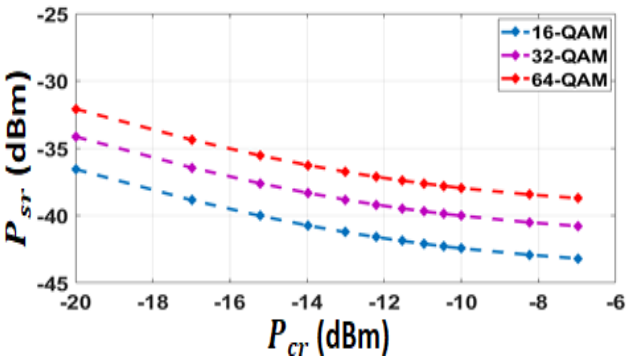

(a)

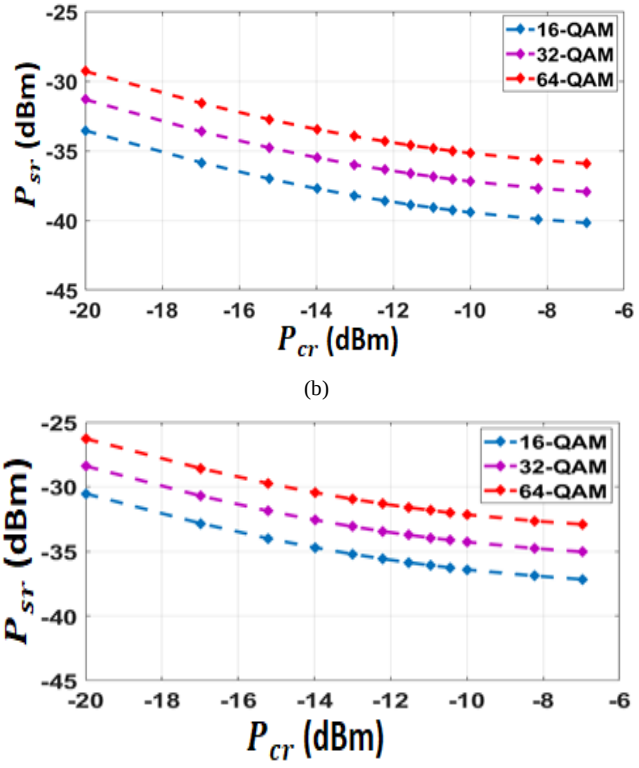

(b)

(c)

Figure 7. Receiver P_{cr}-P_{sr} characteristics when the carrier laser is inserted at the transmitter side. (a) R_b=56 Gbps. (b) R_b=112 Gbps. (c) R_b=224 Gbps

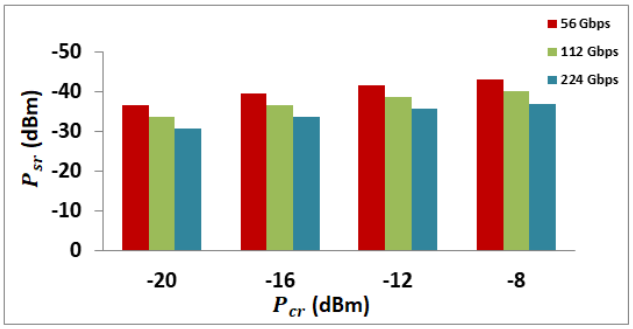

(a)

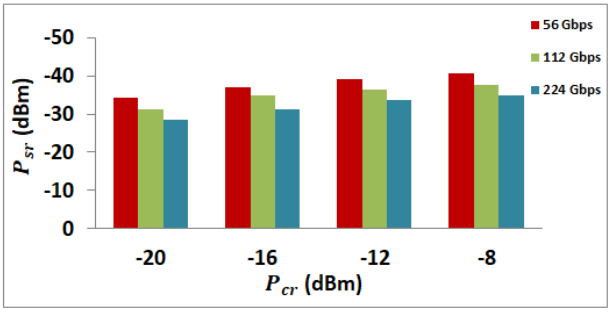

(b)

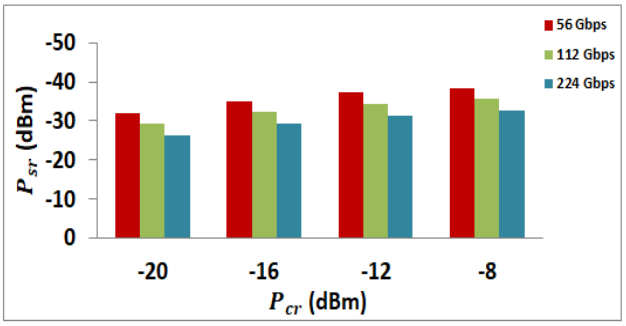

(c)

Figure 8. Values of P_{sr} required to achieve a BER=4.5×10^{-3} at different bit rates. (a) 16-QAM. (b) 32-QAM. (c) 64-QAM

4. Results for Single-Channel System

This section presents simulation results describing the transmission performance of a single-channel NHC communication system operating at 1550 nm wavelength without optical amplification. The system is based on SSB-SCM scheme with optical carrier-assisted technique. The results are reported for both 112 and 224 Gbps data rates and for 16-QAM signaling. Unless otherwise stated, the values of the main system parameters used in the simulation are listed in Table 3. A BER threshold (BER_{th}) of 4.5×10^{-3} is used to estimate the maximum allowable transmission distance L_{max} from the simulation tests.

Table 3. System parameters values used in the simulation for the 16-QAM signaling

Subsystem	Component	Parameter	Value
Transmitter	Signal laser	Frequency f_s	193.1 THz (for 112 and 224 Gbps)
	Carrier laser	Frequency f_c	193.11428 THZ (for 112 Gbps) 193.12856 THZ (for 224 Gbps)
	Mach-Zender optical modulator	Loss	2 dB
	Optical SSB filter	Center frequency	193.08572 THZ (for 112 Gbps) 193.07144 THz (for 224 Gbps)
		Bandwidth	28.56 GHz (for 112 Gbps) 57.12 GHz (for 224 Gbps)
Optical link	Fiber (SSMF)	Attenuation α	0.2 dB/km
		Dispersion D	16.75 ps/nm/km
		Dispersion slop S	0.075 ps/nm^2/km
		Effective area	80 um^2
		Nonlinear index coefficient n_2	26×10^{-21} m^2/W

Subsystem	Component	Parameter	Value
Receiver	Photodiode	Responsibility R	1 A/W
	Front-end electronic amplifier	Load resistance R_L	3.3 kΩ
		Noise Figure F_n	4.8 dB

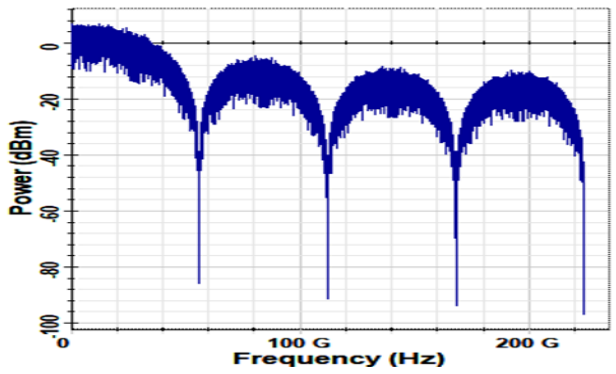

(a)

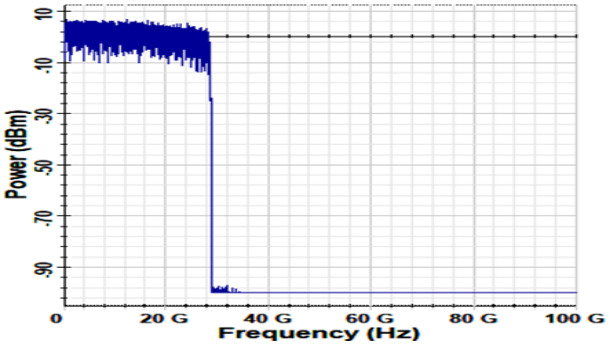

(b)

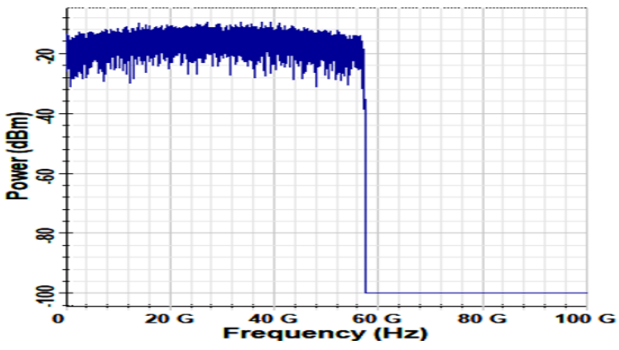

(c)

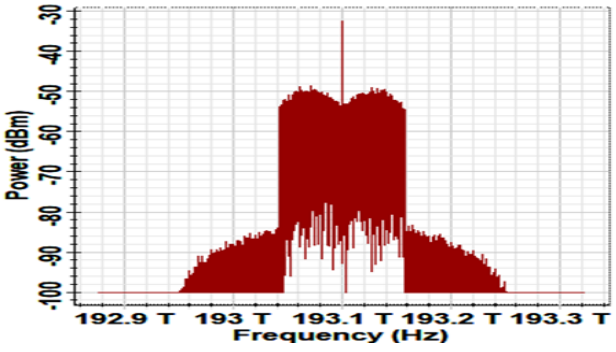

(d)

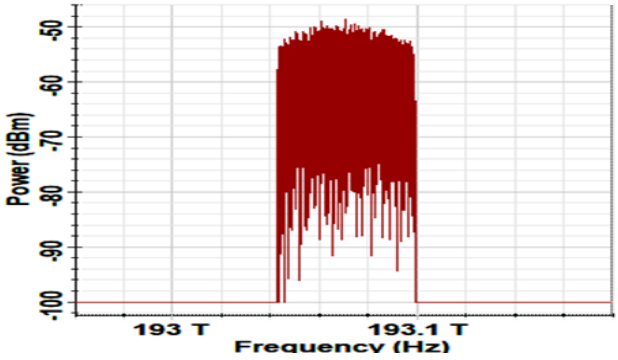

(e)

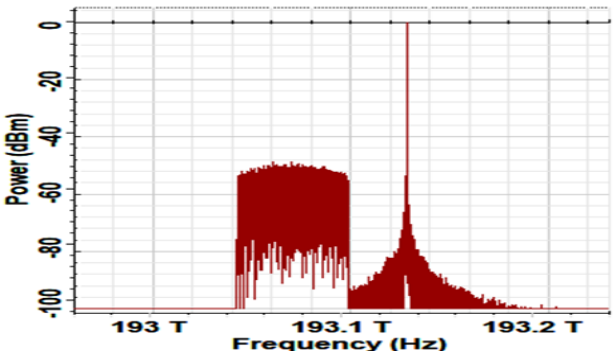

(f)

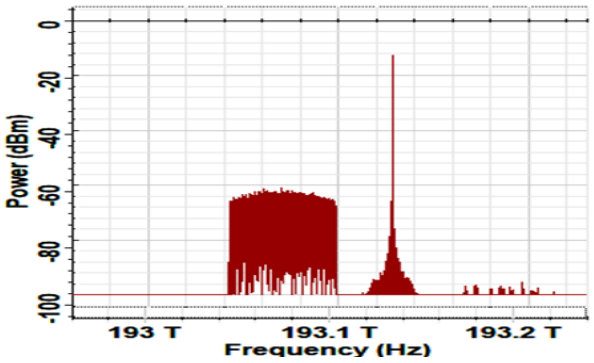

(g)

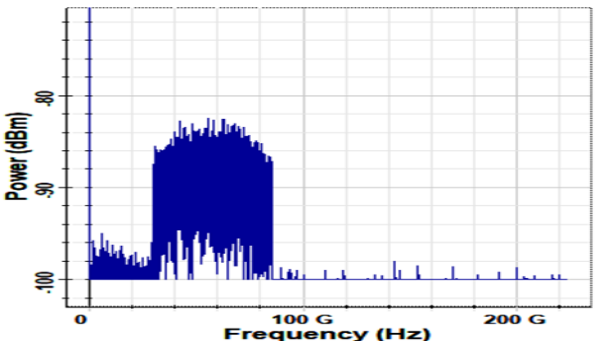

(h)

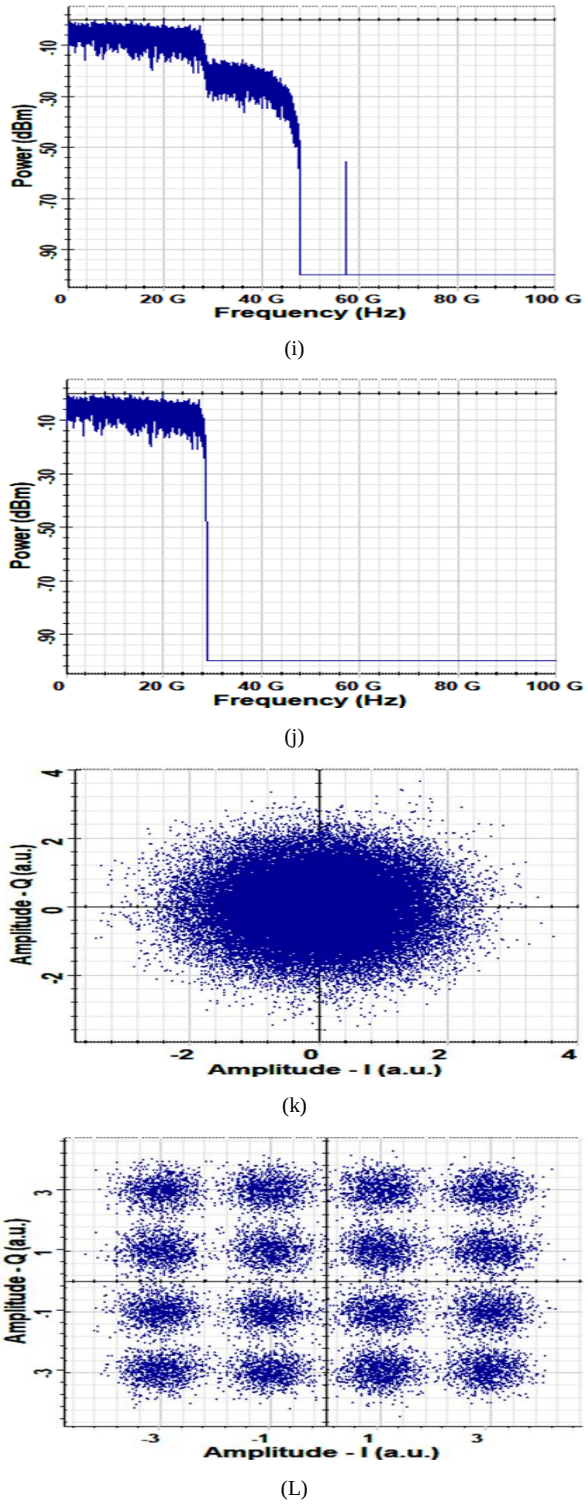

Figure 9. Spectra and constellation diagrams related to 224 Gbps 16-QAM system operating at 1550 nm band with L=62 km, P_s=0 dBm and P_c=0 dBm (carrier at transmitter). (a) Spectrum of the QAM pulse generator output (I-phase component). (b) Spectrum of the QAM modulator input. (c) Spectrum of the QAM modulator output. (d) Spectrum of the optical modulator output. (e) Spectrum of the optical SSB signal. (f) Spectrum of signal SSB + assisted carrier. (g) Spectrum of the optical signal at the fiber output. (h) Spectrum of the amplified photocurrent. (i) Spectrum of the QAM demodulator output. (j) Spectrum of the filtered QAM demodulator output. (k) Receiver constellation diagram at the DSP input. (L) Receiver constellation diagram at the DSP output

4.1. Performance of 224 Gbps System

Figure 9 shows the electrical and optical spectra at different points in the 224 Gbps 16-QAM system. The results are presented for 0 dBm signal laser and 0 dBm carrier laser (inserted in the transmitter side). A 62 km of SSMF is used here which corresponds to L_{max} when P_c=P_s=0 dBm. Figure 9 contains also the receiver constellation diagrams before and after the receiver DSP unit. Figure 9a shows the spectrum of the I-electrical QAM pulse generator. The spectrum contains a baseband component covers the frequency range from 0-56 GHz. Note that the 56 GHz corresponds to the symbol rate R_s=R_b/4. The spectrum also contains high frequency components extending above 56 GHz. The Nyquist shaping filter used in the QAM modulator gives an output electrical signal whose spectrum is limited to R_s/2=28 GHz (see Fig. 9b). The RF QAM modulator uses f_{SCM}=28 GHz and yields a DSB/SC signal at its output whose spectrum extends from 0-56 GHz (see Fig. 9c). This signal is used to modulate the signal laser leading to an optical DSB waveform whose spectrum is illustrated in Fig. 9d. This optical spectrum indicates that there are LSB and USB components (each of 56 GHz bandwidth) in additional to a residual optical carrier. The optical SSB chooses the LSB component (Fig. 9e) which is combined with the carrier laser field using an optical coupler before launching into the fiber input (Fig. 9f). The spectrum of the received optical waveform is given in Fig. 9g and can be considered as a copy of the spectrum at the fiber input except the signal and carrier power levels are reduced due to fiber loss. The peak of the signal and carrier spectrum is reduced by about 12.4 dB after transmission over the 62 km link and this corresponds to the total loss of this link which has 0.2 dB/km attenuation parameter.

Figure 9h displays the spectrum of the amplified photo generated current waveform which has a DSB/SC spectrum around the 56 GHz RF subcarrier with each sideband has 28 GHz bandwidth. The RF QAM demodulator down converts the signal spectrum to the baseband (Fig. 9i) and the required spectrum (0-28 GHz) is obtained after filtering (see Fig. 9j). The constellation diagram at the QAM demodulator output is displayed in Fig. 9k and indicates clearly the presence of random phase effect which comes from the fiber dispersion. The effect of dispersion is compensated using DSP which leads to a clear 16-QAM constellation diagram as shown in Fig. 9L.

The variation of BER with transmission distance L is investigated for the 16-QAM system when P_s=P_c=0 dBm and the results are depicted in Fig. 10. Two curves are plotted in this figure corresponding to two possible locations for inserting the carrier laser, i.e. at the transmitter or receiver side. The figure also contains two receiver constellation diagrams for each case, one is recorded for back to back (B2B) transmission and the other corresponds to L=L_{max} for that case. Note that L_{max} approaches 62 and 78 km when the carrier laser is used at the transmitter and receiver side, respectively. The constellation diagrams at these two distances are almost identical which ensure the same BER

which is 4.5×10.

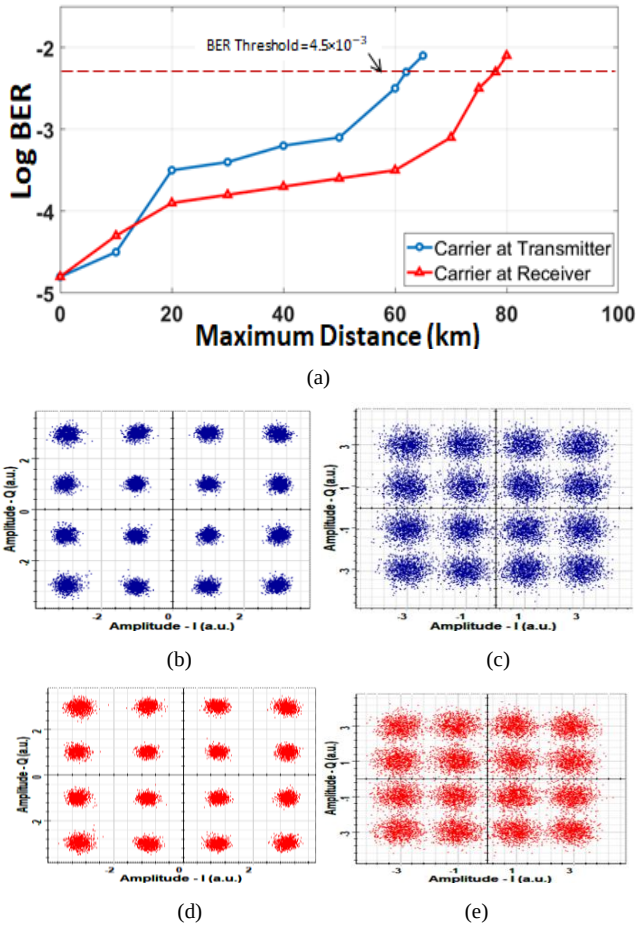

Figure 10. (a) Dependence of BER on transmission distance for 224 Gbps 16-QAM system operating with 0 dBm signal launch power and 0 dBm carrier power. (b) Receiver constellation diagram for B2B transmission (carrier at the transmitter). (c) Receiver constellation diagram after 62 km transmission (carrier at the transmitter). (d) Receiver constellation diagram for B2B transmission (carrier at the receiver). (e) Receiver constellation diagram after 78 km transmission (carrier at the receiver)

Figure 11 shows the variation of the maximum reach L_{max} with signal laser power P_s assuming 16-QAM system operating with P_c=0 dBm. Again two cases related to the location of the carrier laser are considered here. When the carrier laser is used at the transmitter, L_{max} increases slightly with P_s (from 62 km at P_s=0 dBm to 71 km at P_s=6 dBm). When P_s exceeds 6 dBm, L_{max} decreases strongly yielding L_{max} of 45 and 11 km when P_s=8 and 9 dBm, respectively. In contrast, the use of carrier at the receiver side enhances notably the dependence of L_{max} on P_c which is an expected result since the fiber loss does not affect the level of the carrier power used in the receiver detection process. The maximum reach increases from 78 to 102 km (i.e., 24 km change) when P_s increases from 0 to 6 dBm. This change should be compared with 9 km change in the first case. When P_s varies between 7 and 9 dBm, L_{max} approaches almost a saturated level of approximately 107 km. Increasing P_s above 9 dBm leads to decrease in the maximum reach at P_s=10 dBm and L_{max}=49 km.

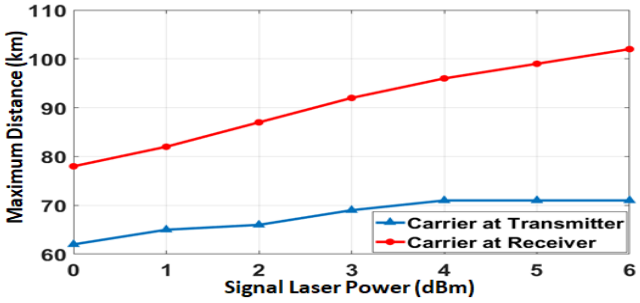

Figure 11. Variation of maximum reach L_{max} with signal laser power P_s assuming 224 Gbps 16-QAM system operating with P_c=0 dBm

The dependence of maximum reach on the carrier power for the 16-QAM system is illustrated in Fig. 12. Parts a-d of this figure are presented for P_s=0, 2, 4, and 6 dBm respectively. Investigation of the results of this figure highlights the following findings

(i) Increasing the carrier laser power beyond 0 dBm has almost negligible effect on the maximum transmission distance when the carrier laser is inserted at the receiver side.

(ii) When the carrier laser is inserted at the transmitter side, then L_{max} increases with increasing P_c and almost reaches the level of L_{max} obtained in the previous case when P_c approaches 10 dBm.

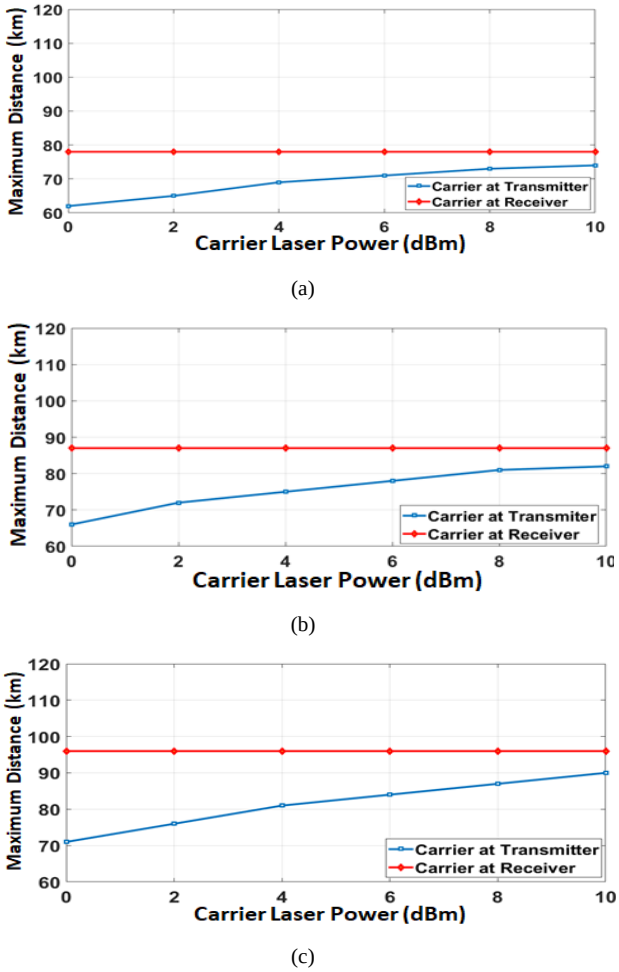

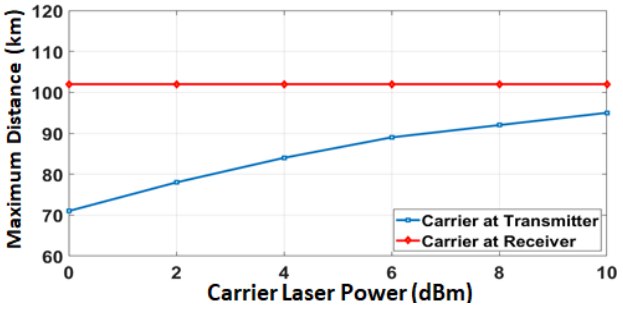

(d)

Figure 12. Dependence of maximum transmission distance on carrier laser power for 224 Gbps 16-QAM system. (a) P_s=0 dBm. (b) P_s=2 dBm. (c) P_s=4 dBm. (d) P_s=6 dBm

The two previous remarks can also be noted from Table 4 which is deduced from Figure 12 and lists the values of L_{max} estimated at P_c=0 and 10 dBm for different values of P_s.

Table 4. Variation of the maximum reach L_{max} with signal laser power P_s assuming 224 Gbps 16-QAM system

Signal Laser Power (dBm)	Maximum Reach (km)			
	Carrier Laser at Transmitter		Carrier Laser at Receiver	
	P_c=0 dBm	P_c=10 dBm	P_c=0 dBm	P_c=10 dBm
0	72	85	92	92
2	77	94	97	97
4	79	100	101	101
6	79	106	119	119

4.2. Performance of 112 Gbps System

Table 5. Variation of the maximum reach L_{max} with signal laser power P_s assuming 112 Gbps 16-QAM system

Signal Laser Power (dBm)	Maximum Reach (km)			
	Carrier Laser at Transmitter		Carrier Laser at Receiver	
	P_c=0 dBm	P_c=10 dBm	P_c=0 dBm	P_c=10 dBm
0	62	74	78	78
2	66	82	87	87
4	71	90	96	96
6	71	95	102	102

The simulation tests of section 4.1 are repeated for 112 Gbps 16-QAM system and the results are adapted in Figs. 13-15 and Table 5. The electrical and optical spectra at different points of the system is given in Fig. 13 and indicate clearly that the transmitter Nyquist shaping filter limits the spectrum of its output waveform to 14 GHz (=R_s/2=R_b/8). When P_s=P_c=0 dBm, the maximum reach is 72 and 92 km depending on the location of the carrier laser (in the transmitter or receiver, respectively), (see Fig. 14). These two values are to be compared with 62 and 78 km for the 224 Gbps counterpart, respectively. Table 5 lists the maximum reach for different values of P_s when P_c=0 and 10 dBm. The table can be used to estimate the optimum value of signal laser power, $(P_s)_{opt}$. The value of $(P_s)_{opt}$ in dBm, when the carrier laser is inserted in the transmission side, gives the highest value of reach, L_{opt}, which equals 79 km. When the carrier laser is used at the receiver side, $(P_s)_{opt}$=8 dBm and gives L_{opt}=122 km. Note that the values of $(P_s)_{opt}$ are almost identical for both 112 and 224 Gbps systems.

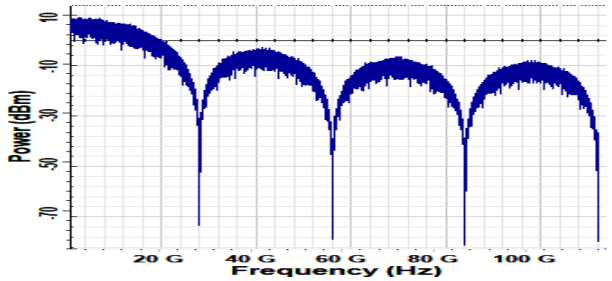

(a)

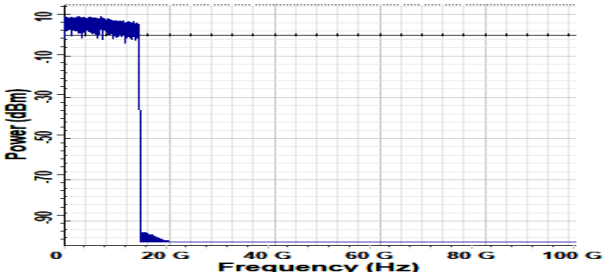

(b)

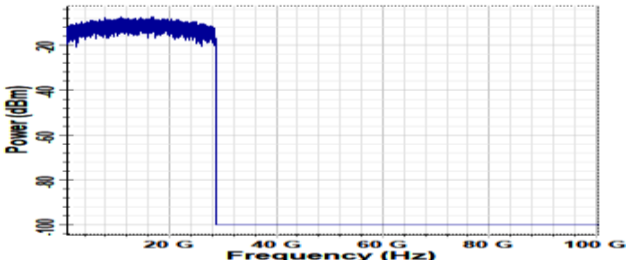

(c)

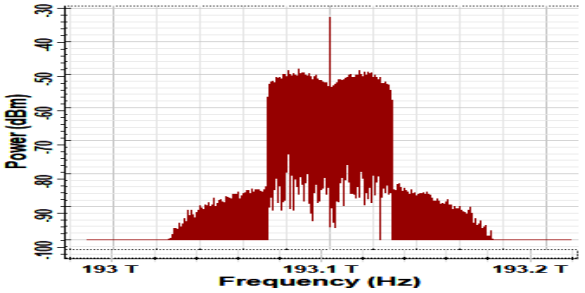

(d)

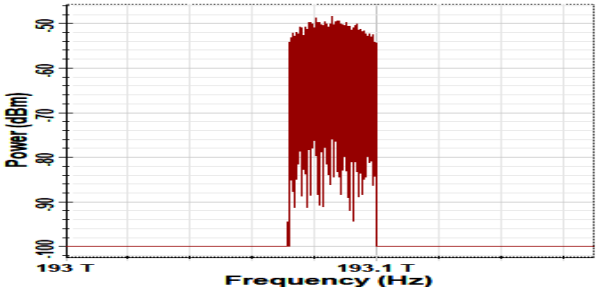

(e)

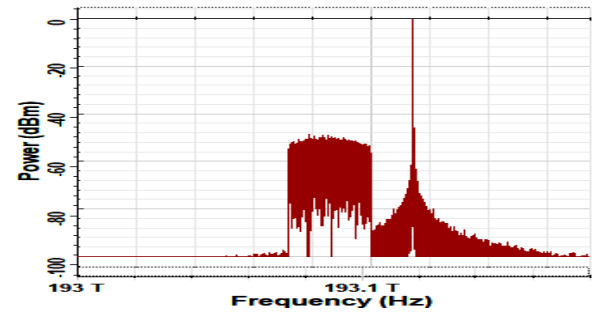

(f)

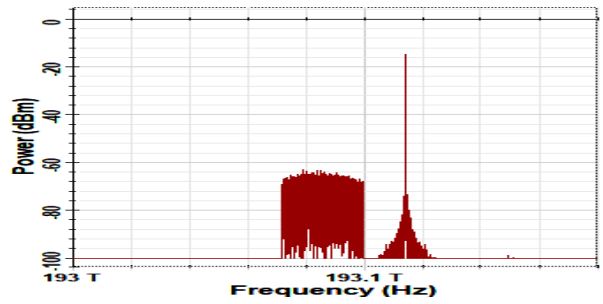

(g)

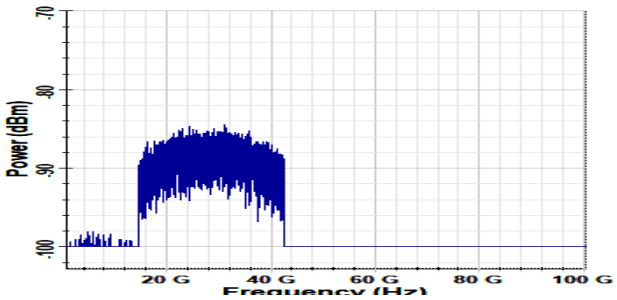

(h)

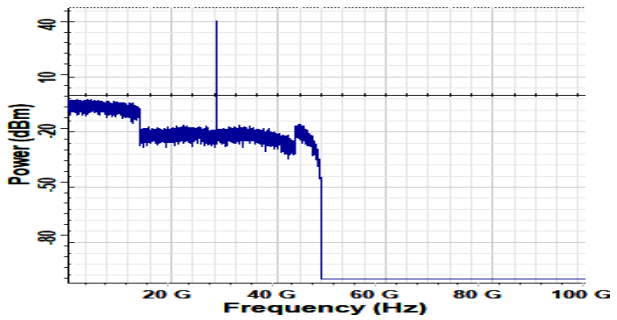

(i)

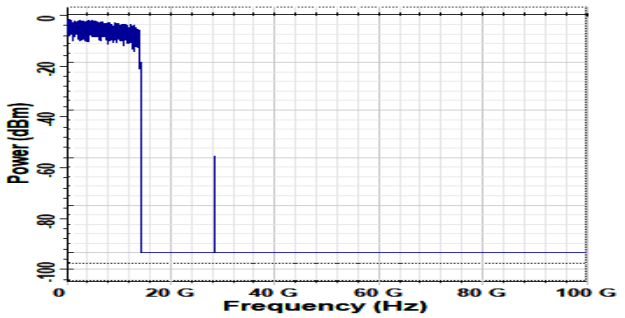

(j)

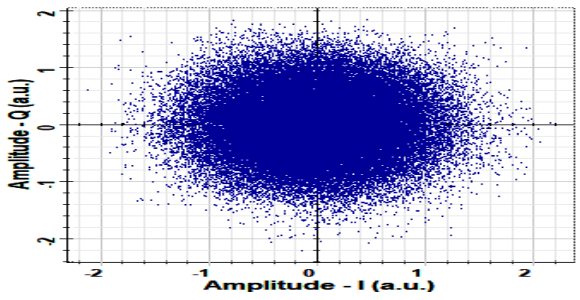

(k)

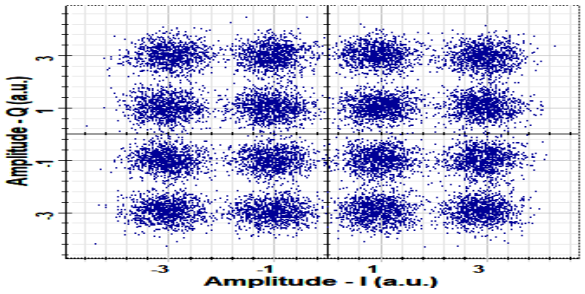

(L)

Figure 13. Spectra and constellation diagrams related to 112 Gbps 16-QAM system operating at 1550 nm band with L=72 km, P_s=0 dBm and P_c=0 dBm (carrier at transmitter). (a) Spectrum of the QAM pulse generator output (I-phase component). (b) Spectrum of the QAM modulator input. (c) Spectrum of the QAM modulator output. (d) Spectrum of the optical modulator output. (e) Spectrum of the optical SSB signal. (f) Spectrum of signal SSB + assisted carrier. (g) Spectrum of the optical signal at the fiber output. (h) Spectrum of the amplified photocurrent. (i) Spectrum of the QAM demodulator output. (j) Spectrum of the filtered QAM demodulator output. (k) Receiver constellation diagram at the DSP input. (L) Receiver constellation diagram at the DSP output

4.3. Summary

Figures 16 and 17 give summary for the transmission performance comparison between the 112 and 224 Gbps 16-QAM system. Figure 16 displays the dependence of the maximum reach on signal power P_s when the carrier laser is in the transmitter side. The simulation is repeated in Fig. 17 assuming the carrier laser is inserted at the receiver side. In both figures, the value of P_s is limited to $(P_s)_{opt}$ corresponding to the case under observation. Investigation of the results of Fig. 16 reveals the following findings. At fixed values of P_c and P_s, the maximum reach of the 112 Gbps system is about 10 km higher than that of 224 Gbps system. When P_s=0 dBm, the highest values of L_{max} equals 85 and 74 km for the 112 and 224 Gbps system, respectively. Thus transmission distance above 100 km cannot be achieved under these conditions. Increasing P_s to 6 dBm increases L_{max} to 106 and 95 km for the 112 and 224 Gbps system, respectively, when P_c=10 dBm. Note further transmission distance above 100 km cannot be achieved for 224 Gbps system. The maximum reach of the 112 Gbps system approaches 100 km when P_s=4 dBm and P_c=10 dBm. When the carrier laser is inserted in the receiver side, the L_{max}-P_s relation becomes almost insensitive to value of P_c. Therefore, Fig. 17 is presented for a simple case (P_c=0 dBm) and indicates that L_{max}=92 and 78 km for 112 and 224 Gbps, respectively, when P_s=0 dBm. Increasing

P_s to 6 dBm increases L_{max} to 119 and 102 km, respectively.

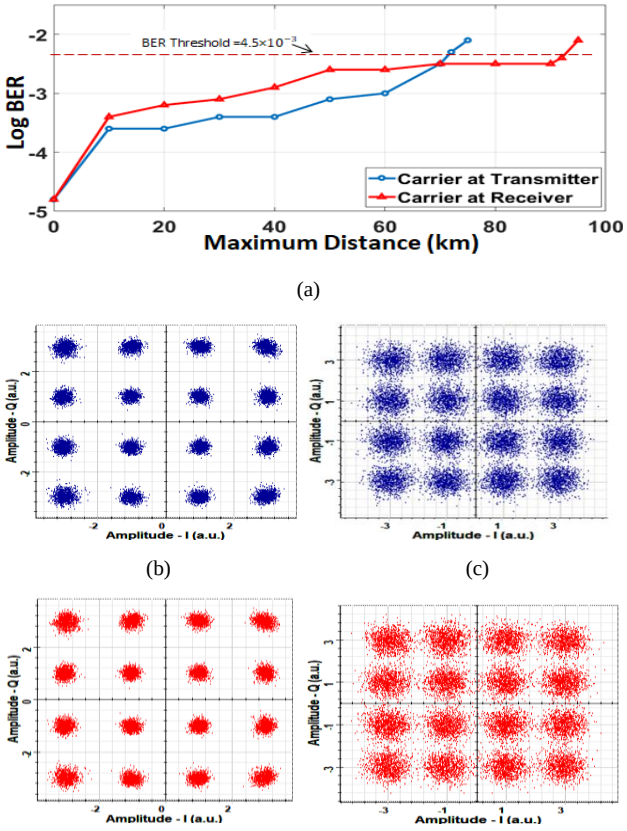

Figure 14. (a) Dependence of BER on transmission distance for 112 Gb/s 16-QAM system operating with 0 dBm signal launch power and 0 dBm carrier power. (b) Receiver constellation diagram for B2B transmission (carrier at the transmitter). (c) Receiver constellation diagram after 72 km transmission (carrier at the transmitter). (d) Receiver constellation diagram for B2B transmission (carrier at the receiver). (e) Receiver constellation diagram after 92 km transmission (carrier at the receiver)

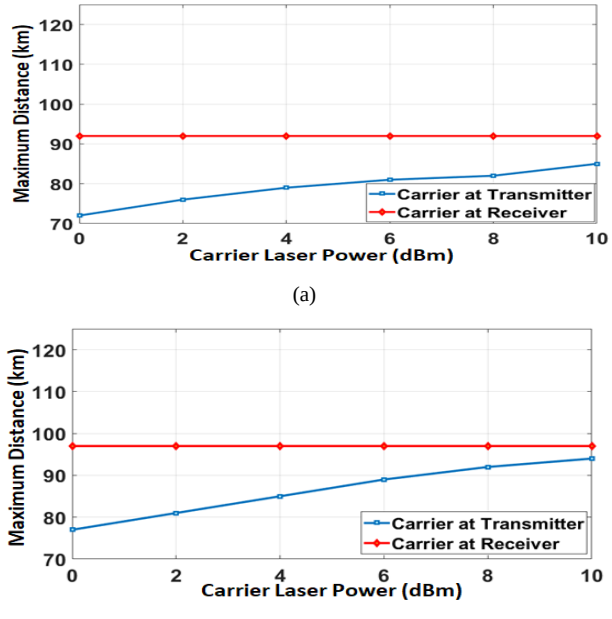

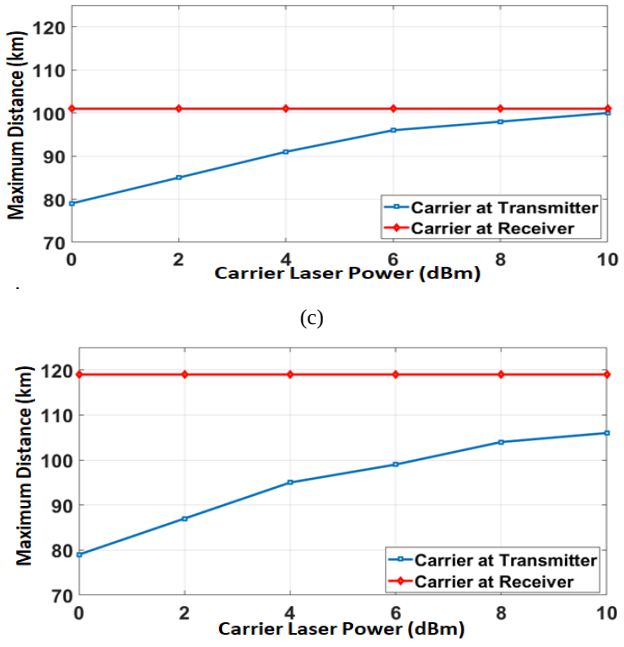

Figure 15. Dependence of maximum transmission distance on carrier laser power for 112 Gbps 16-QAM system. (a) P_s=0 dBm. (b) P_s=2 dBm. (c) P_s=4 dBm. (d) P_s=6 dBm

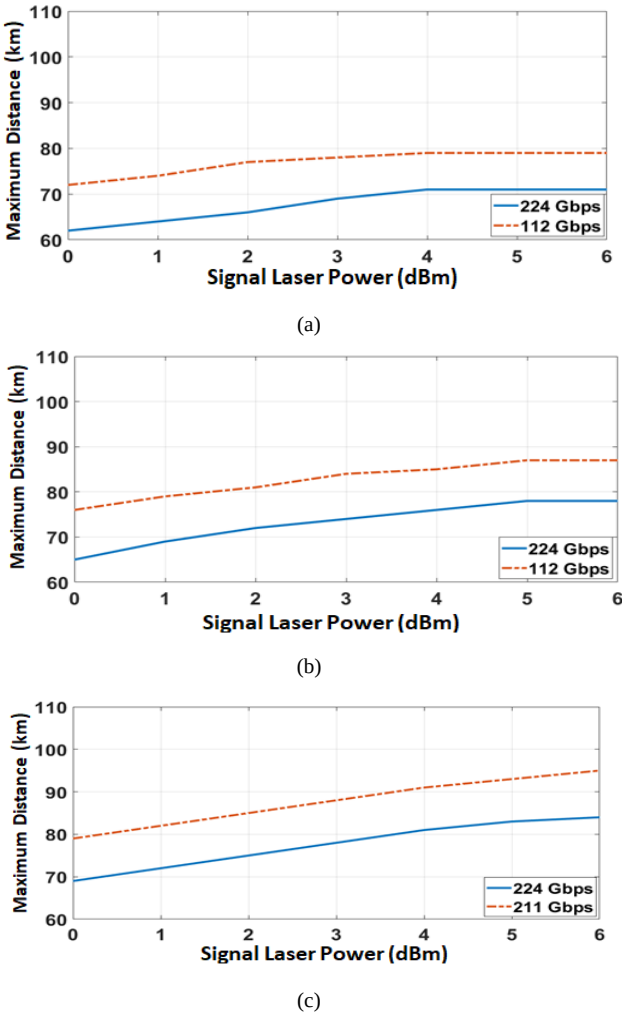

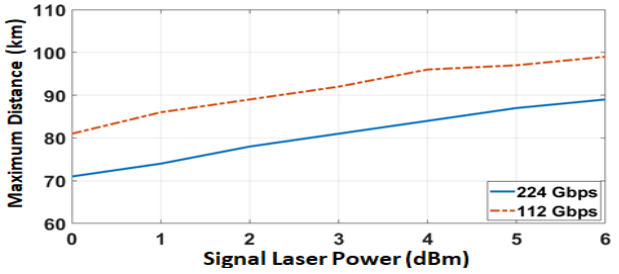

(d)

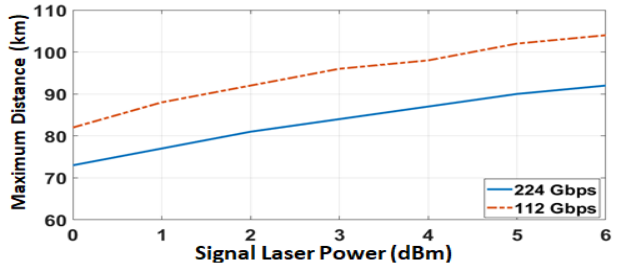

(e)

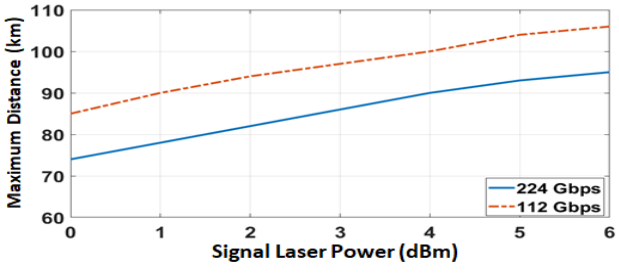

(f)

Figure 16. Variation of maximum distance with signal laser power for 16-QAM system operating with carrier laser inserted at the transmitter side. (a) P_c=0 dBm. (b) P_c=2 dBm. (c) P_c=4 dBm. (d) P_c=6 dBm. (e) P_c=8 dBm. (f) P_c=10 dBm

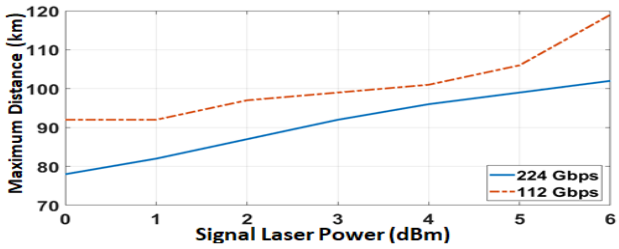

Figure 17. Variation of maximum distance with signal laser power for 16-QAM system operating with 10 dBm carrier laser inserted at the receiver side

5. Capacity Enhancement of NHC System Using Multiplexing Techniques

This section presents feasibility study for enhancing the transmission data rate of NHC system using multiplexing techniques and addressees the transmission performance of the generated multiplexed systems. Both polarization-division multiplexing (PDM) technique, i.e., DP configuration, and WDM technique are used. The results are reported for SSB 16-QAM NHC systems operating at 224 and 112 Gbps per channel without using optical amplification.

5.1. Polarization-Division Multiplexing System

5.1.1. System Configuration

Polarization-division multiplexing technique has been used widely in advanced coherent-detection optical communication systems to double the transmission data rate and hence yields double spectrum efficiency [41, 42]. In this technique, each of two data source is used to modulate one of the two orthogonally polarized components of the laser field. The system is equivalent to transmitting two channels in parallel through the fiber using only one transmitter laser. In coherent optical communication systems, the state of polarization (SOP) of the local laser used in the receiver should match the SOP of the transmitter laser. However, optical fibers suffer from polarization dispersion effect where the two orthogonally polarized optical components do not travel at the same speed on the fiber. This makes the SOP of the received optical signal differs from its SOP at the fiber input. Therefore, matching between the SOPs of the received optical signal and the local laser field should be controlled and updated continuously. This increases the cost and the complexity of the receiver. In this subsection, the concept of PDM is applied to SSB NHC system operating with carrier assisted laser inserted at the transmitter side. Since in this configuration both signal and carrier lasers are at the transmitter, the optical fiber will alter their SOPs by the same amount and therefore, static SOP matching technique can be adopted at the transmitter.

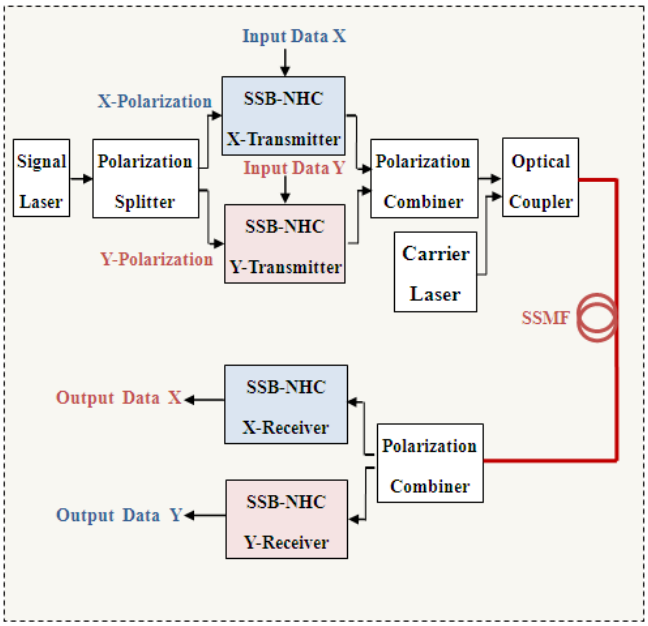

Figure 18. Block diagram of a dual-polarization NHC communication system. SSB: Single side-band; NHC: Nyquist half-cycle

Figure 18 gives a simplified diagram describing the concept of a dual-polarization NHC communication system. The SOPs of both signal and local laser fields are controlled to yield linearly polarized fields with 45° polarization angle. The 45° ensures that the optical powers of the two orthogonal components of each field are equal.

At the transmitter side, the signal laser output enters a polarization beam splitter which produces two orthogonally polarized components (X- and Y-polarization). Each optical component is treated as a signal laser and applied to a SSB NHC transmitter driven by its associated data source. The outputs of both X- and Y-polarization NHC transmitters are combined using a polarization combiner. The resultant optical signal is grouped with the carrier laser output using directional coupler and then launched into the fiber. At the receiver side, the fiber output is applied to a polarization splitter which yields two orthogonally polarized components. The X- (Y-) polarization output component contains both X- (Y-) fields of the received signal and carrier laser. Each of the X- and Y-polarization output of the polarization splitter is applied to a NHC receiver to detect the associated data.

5.1.2. Simulation Results

This subsection presents simulation results related to 2×224 Gbps dual-polarization SSB 16-QAM NHC system operating at the 1550 nm window without optical amplification. Different simulation tests are performed to address the maximum reach corresponding to different values of P_c and P_s. The results reveal that one can get almost the same value of the maximum reach obtained in the 224 Gbps SP counterpart when the signal and carrier lasers powers are doubled. This is clearly noted from Fig. 19 where the maximum reach L_{max} for DP system is plotted versus signal laser power and for different values of carrier laser power. $P_{c\text{-}DP}$ Results corresponding to SP system are also included in this figure for comparison purpose and estimated when both lasers powers are half that of the DP counterpart. [$P_{s\text{-}DP}$=$P_{s\text{-}SP}$+3 (dBm) and $P_{c\text{-}DP}$=$P_{c\text{-}SP}$+3 (dBm)].

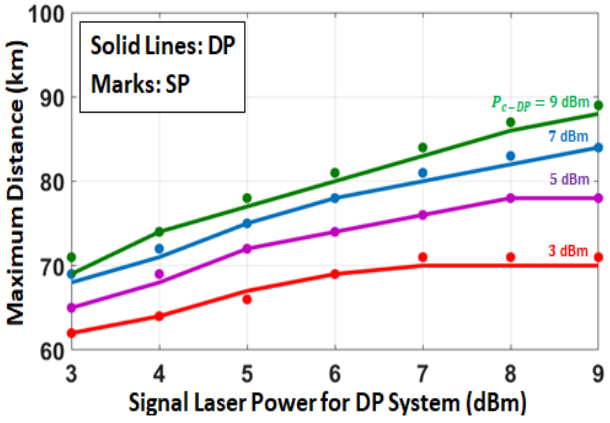

Figure 19. Variation of maximum reach of the 2×224 Gbps dual-polarization 16-QAM system with both signal laser power $P_{s\text{-}DP}$ and carrier laser power $P_{c\text{-}DP}$. The marks correspond to a single-polarization system operates with half the DP lasers powers ($P_{s\text{-}SP}$=0.5 $P_{s\text{-}DP}$ and $P_{c\text{-}SP}$=0.5 $P_{c\text{-}DP}$)

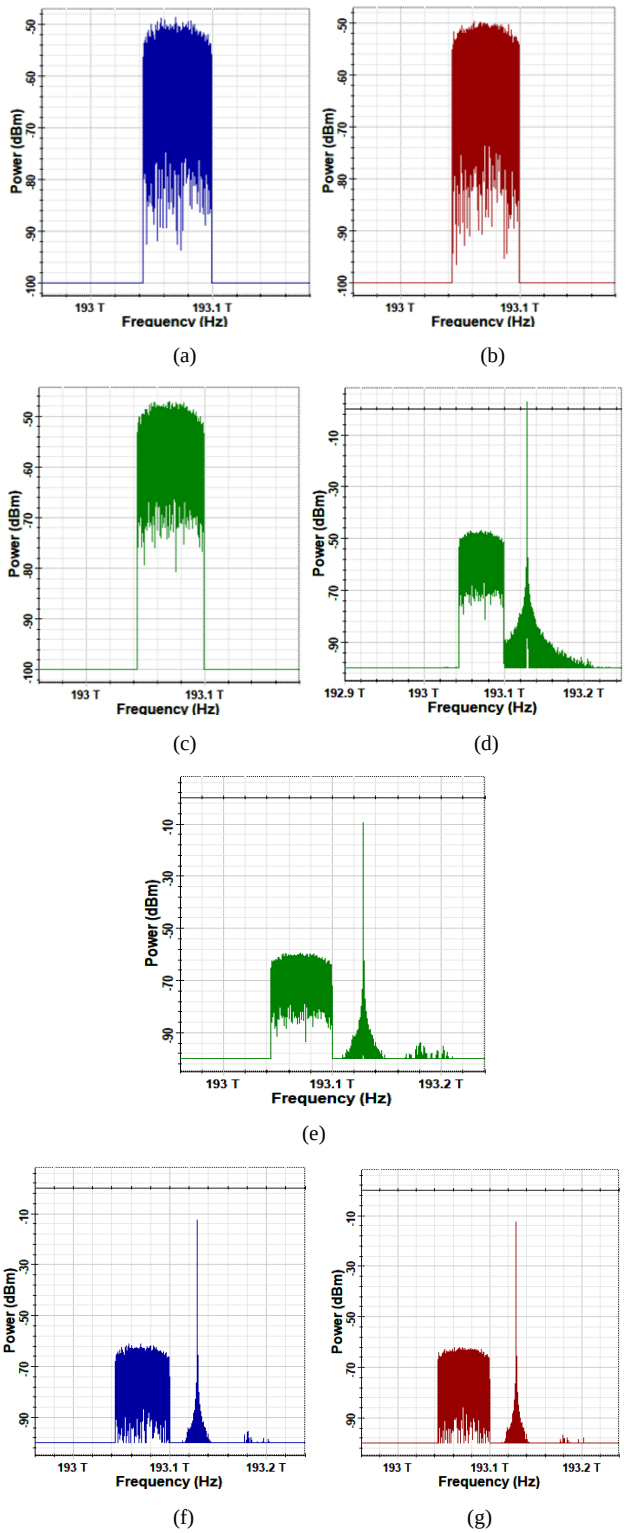

Figure 20. Spectra and constellation diagrams related to 2×224 Gbps DP 16-QAM system operating at 1550 nm with L=62 km, P_s=3 dBm and P_c=3 dBm (carrier at transmitter). (a) Spectrum of the signal at the X-transmitter output. (b) Spectrum of the signal at the Y-transmitter output. (c) Spectrum of the signal at the output of the transmitter polarization combiner. (d) Spectrum of the optical signal at the fiber input. (e) Spectrum of the optical signal at the fiber output. (f) Spectrum of the received signal at the X-receiver. (g) Spectrum of the received signal at the Y-receiver. (h) Receiver constellation diagram at the DSP output at the X-receiver. (i) Receiver constellation diagram at the DSP output at the Y-receiver

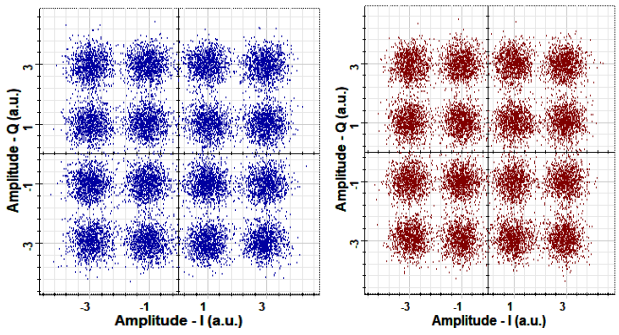

(h) (i)

Figure 20. (Continued)

It is clear from the results of Fig. 19 that the DP system under investigation behaves as two parallel systems sharing equally the total bit rate and transmitted along the fiber without interaction between them. This is illustrated further in Fig. 20 where the power spectra at different points are recorded along with receiver constellation diagrams for the PDM 16-QAM system operating with 448 Gbps (2×224 Gbps) data rate over 62 km of SSMF. The signal laser power is set to 3 dBm and assumed equals the carrier laser power. The 62 km corresponds to the maximum reach under these conditions. Figures 20a-c shows the power spectra of the signals at the X-transmitter output, Y-transmitter output, and the output of the transmitter polarization combiner. Note that the spectra occupy the same bandwidth (=56 GHz). The spectra of the waveforms at the fiber input and output are illustrated in Figs. 20d and 20e, respectively. The spectra of the received optical signals corresponding to the X-receiver and Y-receiver are given in Figs. 20f and 20g, respectively, which are identical in both amplitude and frequency contents. The constellation diagrams for both receivers are given in Figs. 20h and 20j. Note that the figures of the X-polarization channel match that of the Y-polarization channel.

5.2. Nyquist-Half Cycle WDM System

This subsection investigates the possibility of using WDM technique to enhance the capacity of SSB 16-QAM NHC system operating with 112 or 224 Gbps per channel data rate. The WDM system operating in the C-band using unamplified SSMF link.

5.2.1. System Configuration and Design Issues

Figure 21 shows a simplified block diagram for the NHC WDM system under investigation. Each channel operates with OCA-scheme where the carrier laser is inserted in the optical receiver. Inserting the carrier laser in the channel transmitter side is almost impossible due to the presence of neighbouring optical channels. The N-channel WDM transmitter consists of N SSB NHC single-channel transmitters, each operates with its own signal laser and signal date. The N signal lasers have different C-band wavelengths but with fixed frequency channel spacing Δf. The center frequency of the optical SSB filter in each NHC channel transmitter is adapted according to the symbol rate and signal laser frequency of that channel. The bandwidth of this filter is identical for all channels and set to the symbol rate R_s.

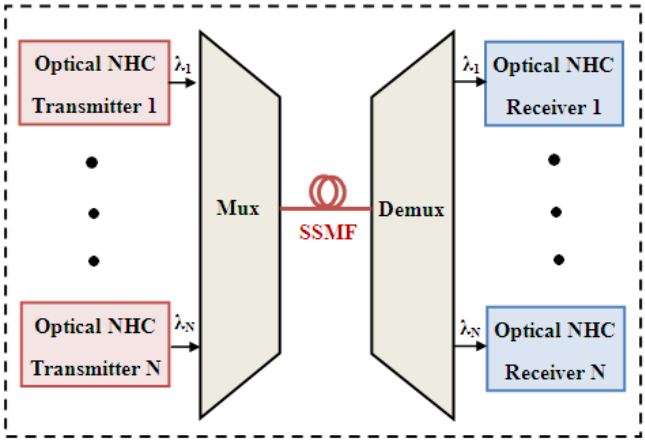

Figure 21. Block diagram of SSB NHC-based wavelength division multiplexing communication system

The optical outputs of the N transmitters are grouped together using multiplexer and the resultant output waveform is lunched into the fiber. The optical waveform at the fiber end enters a demultiplexer who works on frequency-domain platform and acts as a wavelength-selective splitter. Each of the N outputs of the splitter is applied to one of the N OCA-receivers. Each receiver is design according to channel wavelength and supported by its own carrier laser.

The frequency channel spacing Δf should be chosen to ensure negligible overlapping between the spectra of neighboring channels. This helps the demultiplexer at the receiver side to select the required channel with negligible crosstalk. The International Telecommunication Union-Telecommunication Standardization Sector (ITU-T) has issued a C-band frequency grid which specifies the frequencies of the laser sources that can be used in the WDM system [38]. The grid is based on Δf=50 GHz and the laser frequencies are distributed around a center frequency of 193.1 THz (≈ 1550 nm). For practical WDM system, the designer must choose the laser frequencies from this grid with specific Δf that ensures negligible crosstalk at the demultiplexer output (i.e., Δf=50, 100, or 150 GHz).

The spectrum bandwidth of the SSB 16-QAM NHC transmitter is limited to $R_s/4$ and therefore, equal 56 and 28 GHz when 224 and 112 Gbps date rates are used, respectively. The channel spacing Δf must be chosen higher than that. In this work Δf is set to 100 and 50 GHz for 224 and 112 Gbps channel data rates, respectively. In the following simulation, the frequency of the ith channel signal laser f_i is computed according to eqn. 22

$$f_i(\text{THz})=193.1+[i-(1+N/2)]\Delta f(\text{THz}) \quad (22)$$

where i=1, 2,…, N. Note that the (1+N/2) is the center channel whose laser frequency is 193.1 THz. For N=4, 8, 16, and 32 WDM systems. The center channels are 3, 5, 9, and 13, respectively.

5.2.2. Simulation Results

Simulation results are presented here for SSB 16-QAM NHC system operating with 4-, 8-, 16-, and 32- channel WDM techniques and supported by 0 dBm-OCA scheme. The value of P_c does not affect the maximum reach since the carrier is inserted in the receiver side. The results are reported for both 112 and 224 Gbps channel data rates.

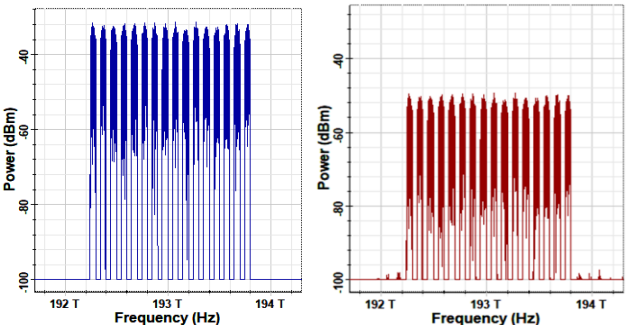

Figure 22. Optical power spectra corresponding to 16×224 Gbps WDM system operating with 16-QAM signal and P_s=6 dBm. (a) At the fiber input. (b) After 90 km transmission

The transmission performance of WDM communication systems is usually affected by fiber nonlinear optics and it is mainly due to the dependence of fiber core refractive index on the total intensity of light passing through it and also due to nonlinear fiber scattering effects [4, 10, 43]. In contrast, simulation tests performed on the WDM system under investigation reveal that the effect of fiber nonlinearities are almost negligible even with 16-channel system operating with channel signal laser having 6 dBm power. The reason behind that is that the power of the optical SSB NHC transmitter is much less than the corresponding signal laser power. For example, consider the 16-channel WDM system operating with P_s=6 dBm, 224 Gbps channel data rate, and 16-QAM signaling. The optical modulator used in the system is based on dual-port Mech-Zehnder (MZM) configuration having 2 dB insertion loss. The modulator generates a double-side band (DSB) signal of -6.4 dBm power. The SSB filter chooses one SSB and yields an output signal of -9.5 dBm which is almost half the DSB signal power. The optical power of the WDM waveform at the multiplexer output (which represent the total power launched into the fiber) is found to be 2.5 dBm from the simulation and it corresponds to (-9.5+10log16) dBm. This level of total launch power is relatively low and cannot enhance the effect of nonlinear fiber optics. This conclusion can be deduced from Fig. 22 which compares the optical spectrum of the 16-channel WDM signal at the fiber input with that after 90 km transmission. The results are reported for a system operating with P_s=6 dBm, 16-QAM signaling, and 224 Gbps channel data rate. Note that the signal spectrum at the fiber output matches that at the fiber input from the frequency contents point of view. The level of transmitted signal reduces by 18 dB across the 90 km fiber due to fiber loss (0.2 dB/km).

When the signal laser power in the previous example increases to 8 dBm, the launch power will increase to 4.5 dBm and the effect of fiber nonlinear optics become more pronounced. This is illustrated in Fig. 23 where the optical spectra at the input and output of 90 km SSMF are recorded. Note that the optical signal at the fiber end contains many distortion components introduced by the fiber nonlinearity. When the nonlinearity parameters in the used software are tuned to zero, the distortion components disappear as shown in Fig. 23c.

The effect of nonlinear fiber optics is more clear with the 32-channel system. At P_s=6 dBm, the optical power of the multiplexer output is 5.5 dBm (=-9.5+10log32). Figure 24 shows the corresponding optical spectrum at the input and output of 75 km fiber. More distortion components appeared at the fiber output compared with case of 16-channel WDM system. The simulation results revel that the maximum reach of 32-channel system operating with P_s=6 dBm is limited to 75 km compares with 90 km for the 16-channel system.

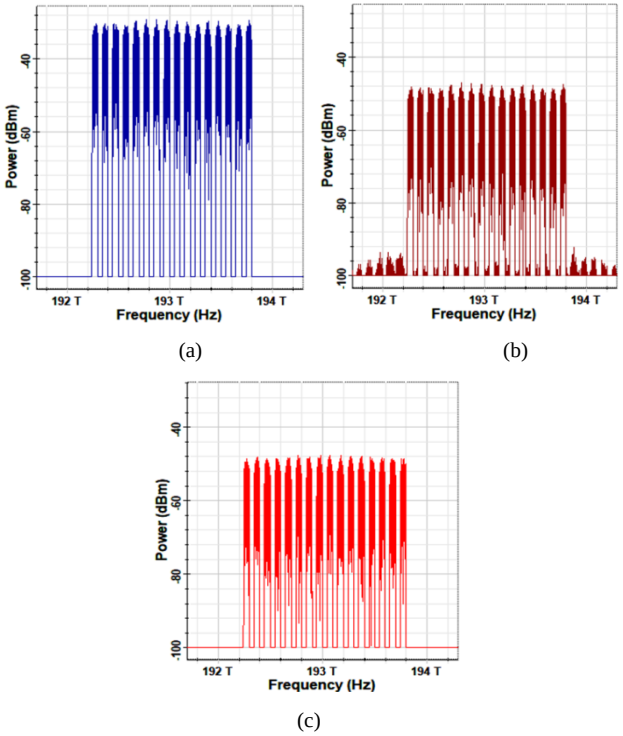

Figure 23. Optical power spectra corresponding to 16×224 Gbps WDM system operating with 16-QAM signal and P_s= 8 dBm. (a) At the fiber input. (b) After 90 km transmission in the presence of fiber nonlinear optics. (c) After 90 km transmission in the absence of fiber nonlinear optics

Figure 25 illustrates the dependence of maximum reach for 16-QAM WDM system on signal laser power and assuming P_c=0 dBm and channel data rate of 224 Gbps. The results are given for four WDM systems having 4, 8, 16, and 32 channels. Results related to a single-channel counterpart are also included in the figure for comparison purposes. Note that the maximum reach is almost independent of number of multiplexed channels when N=1, 4, and 8. Increasing N to 16 or 32 reduces L_{max} compared with, N=1, 4 and 8 systems and this effect is more pronounced with increasing P_s. For

example, L_{max} corresponding to P_s=0 dBm equals 78, 77, 75, 72, and 65 km when N=1, 4, 8, 16, and 32, respectively. Increasing P_s to 8 dBm yields L_{max}=108, 108, 108, 90, and 60 km, respectively.

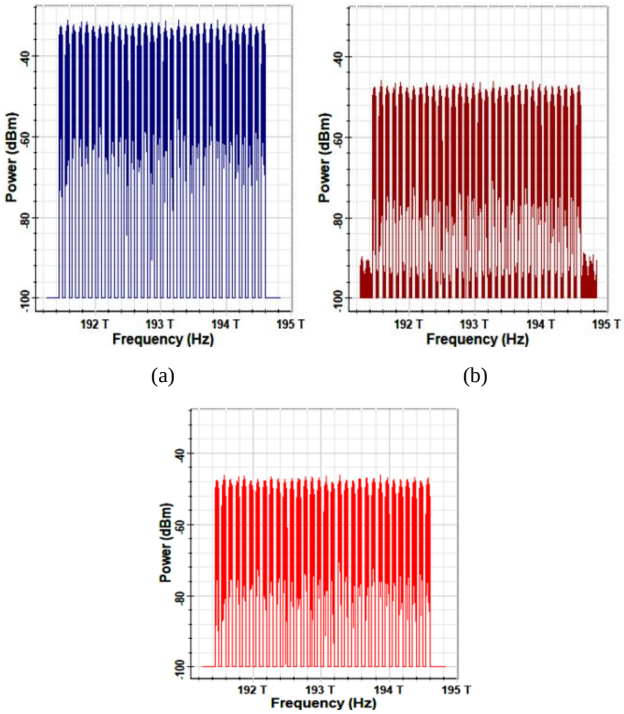

Figure 24. Optical power spectra corresponding to 32×224 Gbps WDM system operating with 16-QAM signal and P_s=6 dBm. (a) At the fiber input. (b) After 75 km transmission in the presence of fiber nonlinear optics. (c) After 75 km transmission in the absence of fiber nonlinear optics

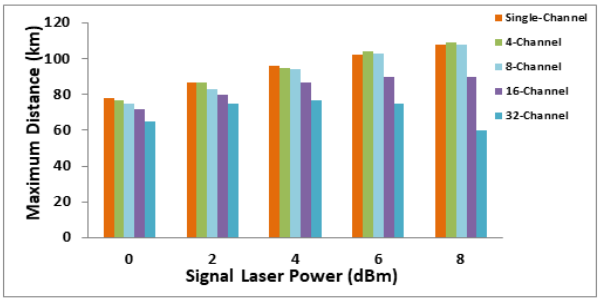

Figure 25. Dependence of maximum reach of 16-QAM WDM system on signal laser power and assuming P_c=0 dBm and channel data rate=224 Gbps

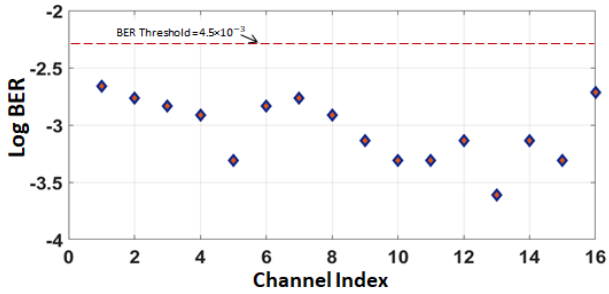

Figure 26. Variation of BER with channel index for 16-channel WDM system operating with P_c=0 dBm, P_s=6 dBm, R_b=224 Gbps per channel, L=90 km, and 16-QAM signaling

An example of variation of BER among various WDM channels is given in Fig. 26 assuming N=16, P_c=0 dBm, P_s=6 dBm, R_b=224 Gbps per channel, and L=90 km. The 90 km fiber length represents the maximum reach L_{max} for this system. Note that the BERs of all the sixteen channels are lower than BER threshold (=4.5×10^{-3}).

The simulation is carried further to investigate the transmission performance of the WDM system operating with 112 Gbps channel data rate and 16-QAM signaling. The results are depicted in Fig. 27 for different values of channel power P_s and assuming P_c=0 dBm. The corresponding optical spectra under different operating conditions are given in Appendix and ensure that the effect of nonlinear fiber optics is relatively less pronounced compared with the 224 Gbps WDM counterpart. Table 6 lists comparison between the transmission performance of N×112 and N×224 Gbps WDM system. The table gives the bit rate-maximum distance product as a function of signal laser power and number of multiplexed channels N.

Table 6. Comparison between the transmission performance of N×112 and N×224 Gbps WDM system

(a) Channel data rate = 112 Gbps.

Signal Laser Power(dBm)	Data Rate-Maximum Reach Product ($Tbps^{-1}km$)				
	N=1	N=4	N=8	N=16	N=32
0	92	92	86	86	86
2	97	97	94	93	90
4	101	101	101	93	90
6	119	119	108	80	78
8	112	112	104	72	70

(b) Channel data rate = 224 Gbps.

Signal Laser Power(dBm)	Data Rate-Maximum Reach Product($Tbps^{-1}km$)				
	N=1	N=4	N=8	N=16	N=32
0	78	77	75	72	65
2	87	87	83	80	75
4	96	95	94	87	77
6	102	104	103	90	75
8	108	109	108	90	60

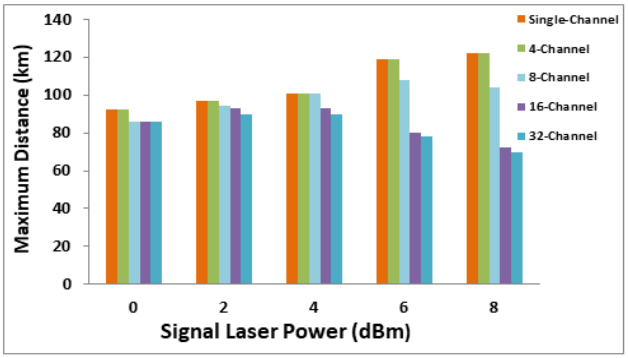

Figure 27. Dependence of maximum reach of 16-QAM WDM system on signal laser power and assuming P_c=0 dBm and channel data rate of 112 Gbp

Appendix Optical Spectra for 112 Gbps

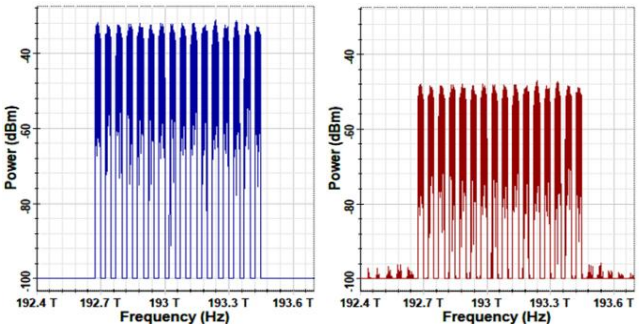

(a) (b)

Figure 28. Optical power spectra corresponding to 16×112 Gbps WDM system operating with 16-QAM signal and P_s=6 dBm. (a) At the fiber input. (b) After 80 km transmission

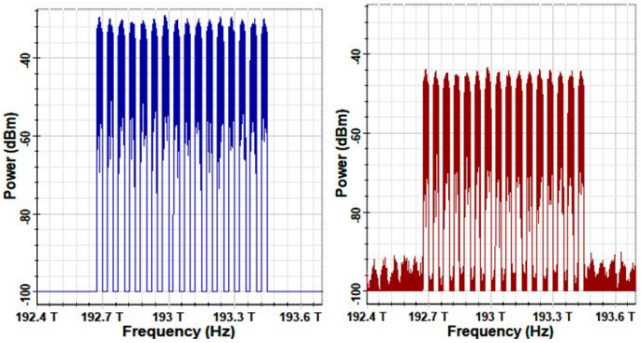

(a) (b)

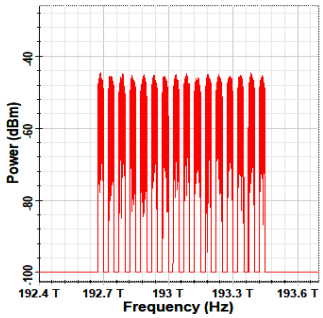

(c)

Figure 29. Optical power spectra corresponding to 16×112 Gbps WDM system operating with 16-QAM signal and P_s=8 dBm. (a) At the fiber input. (b) After 72 km transmission in the presence of fiber nonlinear optics. (c) After 72 km transmission in the absence of fiber nonlinear optics

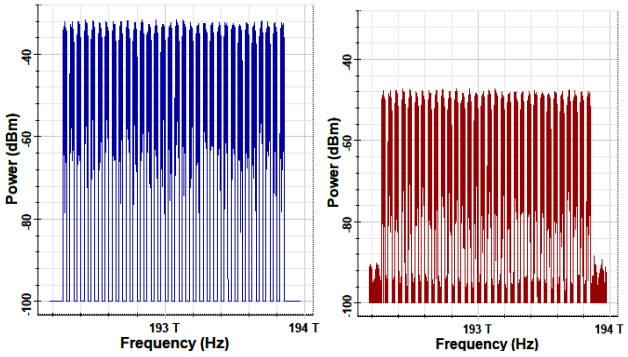

(a) (b)

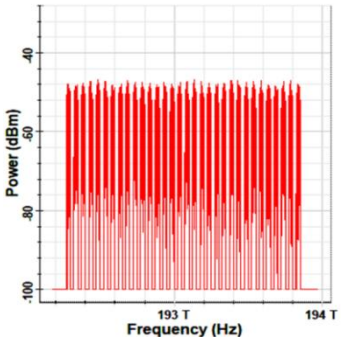

(c)

Figure 30. Optical power spectra corresponding to 32×112 Gbps WDM system operating with 16-QAM signal and P_s=6 dBm. (a) At the fiber input. (b) After 78 km transmission. (c) After 78 km transmission in the absence of fiber nonlinear optics

6. Conclusions

The BER characteristics and transmission performance of unamplified optical carrier assisted NHC-SSB system have been investigated numerically and by simulation. Results have been presented for 16-QAM 1550 nm single-channel and C-band multichannel transmission with channel data rate up to 224 Gbps. The main conclusions of this study are

(i) Doubling the bit rate of a given signaling format increase the receiver sensitivity by about 3 dBm.

(ii) For giving bit rate, going from 16-QAM to 32-QAM increases the receiver sensitivity by about 2.4 dB. This is to be compared with about 2.3 dB when one goes from 32-QAM to 46-QAM signaling.

(iii) The maximum reach L_{max} channel increases slightly with signal laser power when the carrier laser is inserted at the transmitter side. (for 62 km at P_s=0 dBm to 71 km at P_s=6 dBm when the carrier laser power P_c=0 dBm). Using the carrier laser at the receiver side increases L_{max} notably. (From 78 to 102 km when P_s increases from 0 to 6 dBm).

(iv) The effect of fiber nonlinear optics almost negligible for the NHS-SSB WDM system.

(v) With P_s=P_c=0 dBm, L_{max} equals 86 km for the 32×112 Gbps system and 65 km for the 32×224 Gbps system.

REFERENCES

[1] J. Zhang, J. Yu, Y. Fang, and N. Chi, "High speed all optical Nyquist signal generation and full-band coherent detection", Scientific Reports, vol. 4, Article no. 6156, pp. 1-8, Aug. 2014.

[2] S. Chen, C. Xie, and J. Zhang, "Comparison of advanced detection techniques for QPSK signals in super-Nyquist WDM systems", IEEE Photonics Technology Letters, vol. 27, no. 1, pp. 105-108, Jun. 2015.

[3] J. Zhang, Y. Zheng, X. Hong, and C. Guo, "Increase in

capacity of an IM/DD OFDM PON using super-Nyquist image-induced aliasing and simplified nonlinear equalization", IEEE Journal of Lightwave Technology, vol. 35, no. 19, pp. 4105-4113, Oct. 2017.

[4] D. Soma, Y. Wakayama, S. Beppu, S. Sumita, and T. Tsuritani, "10.16-Peta-B/s dense SDM/WDM transmission over 6-mode 19-core fiber across the C+L band", IEEE Journal of Lightwave Technology, vol. 36, no. 6, pp. 1362-1368, Mar. 2018.

[5] O. A. Sab, P. Plantady, A. Calsat, S. Dubost, L. Schmalen, V. Letellier, and J. Renaudi, "25.4-Tb/s transmission over transpacific distances using truncated probabilistically shaped PDM-64QAM", IEEE Journal of Lightwave Technology, vol. 36, no. 6, pp. 1354-1361, Mar. 2018.

[6] W. Patterson, A. Turukhin, M. Bolshtyansky, and D. Foursa, "51.5 Tb/s capacity over 17,107 km in C+L bandwidth using single-mode fibers and nonlinearity compensation", IEEE Journal of Lightwave Technology, vol. 36, no. 11, pp. 2135-2141, Jun. 2018.

[7] J. Weerdenburg, S. Member, R. Ryf, and C. Okonkwo, "138-Tb/s mode- and wavelength-multiplexed transmission over six-mode graded-index fiber", IEEE Journal of Lightwave Technology, vol. 36, no. 6, pp. 1369-1374, Mar. 2018.

[8] D. Soma, S. Beppu, Y. Wakayama, K. Igarashi, and M. Suzuki, "257-Tbit/s weakly coupled 10-mode C + L-band WDM transmission", IEEE Journal of Lightwave Technology, vol. 36, no. 6, pp. 1375-1381, Mar. 2018.

[9] S. S. Kashef and P. Azmi, "Performance analysis of nonlinear fiber-optic in CO-OFDM systems with high order modulations", IEEE Photonics Technology Letters, vol. 30, no. 8, pp. 696-699, Apr. 2018.

[10] P. Morel, M. Morvan, P. Gravey, and E. Pincemin, "Sparse preamble design for polarization division multiplexed CO-OFDM/OQAM channel estimation", IEEE Journal of Lightwave Technology, vol. 36, no. 13, pp. 2737-2745, Jul. 2018.

[11] A. Tanaka, S. Murakami, T. Tajima, T. J. Xia, and G. A. Wellbrock, "Terabit/s Nyquist super channels in high capacity fiber field trials using DP-16QAM and DP-8QAM modulation formats", IEEE Journal of Lightwave Technology, vol. 32, no. 4, pp. 776-782, Feb. 2014.

[12] M. Nakao, T. Ishihara, and S. Sugiura, "Dual-mode time-domain index modulation for Nyquist-criterion and faster-than-Nyquist single-carrier transmissions", IEEE Access, vol. 5, pp. 27659 -27667, Nov. 2017.

[13] S. Peng, A. Liu, X. Pan, and H. Wang, "Hexagonal multicarrier faster-than Nyquist signaling", IEEE Access, vol. 5, pp. 3332- 3339, Mar. 2017.

[14] K. Zou, Y. Zhu, F. Zhang, and Z. Chen, "200Gbit/s Nyquist 16-QAM half-cycle subcarrier modulation transmission with dual-polarization direct detection", 21st OptoElectronics and Communications Conference/International Conference on Photonics in Switching (OECC/PS), pp. 3-7, Jul. 2016.

[15] L. Sheikh, A. G. i Amat, and G. Liva, "Achievable information rates for coded modulation with hard decision decoding for coherent fiber-optic systems", IEEE Journal of Lightwave Technology, vol. 35, no. 23, pp. 5069-5078, Dec. 2017.

[16] Lin Jiang, L. Yan, A. Yi, Y. Pan, M. Hao, W. Pan, and B. Luo, "Chromatic dispersion, nonlinear parameter, and modulation format monitoring based error for coherent optical transmission systems", IEEE Photonics Journal, vol. 10, no. 1, Article no. 7900512, Feb. 2018.

[17] P. Runge, G. Zhou, W. Ebert, S. Mutschall, A. Seeger, and M. Schell, "Waveguide integrated balanced photodetectors for coherent receivers", IEEE Journal of Selected Topics in Quantum Electronics, vol. 24, no. 2, Article no. 6100307, Mar./Apr. 2018.

[18] M. Chagnon, M. M. Osman, and D. V. Plant, "Half-terabit single-carrier direct-detect transceiver, formats, and DSP: analysis and demonstration", IEEE Journal of Lightwave Technology, vol. 36, no. 2, pp. 447-459, Jan. 2018.

[19] Z. Li, E. Sillekens, L. Galdino, T. Xu, B. C. Thomsen, P. Bayvel, and R. I. Killey, "Digital linearization of direct-detection transceivers for spectrally-efficient 100 Gb/s/λ WDM metro networking", IEEE Journal of Lightwave Technology, vol. 36, no. 1, pp. 27-36, Jan. 2018.

[20] S. T. Le , K. Schuh, M. Chagnon, F. Buchali, R. Dischler, V. Aref, H. Buelow, and K. M. Engenhardt, "1.72-Tb/s virtual-carrier-assisted direct-detection transmission over 200 km", IEEE Journal of Lightwave Technology, vol. 36, no. 6, pp. 1347-1353, Mar. 2018.

[21] J. Tang, J. He, D. Li, M. Chen, and L. Chen,"64/128-QAM half-cycle subcarrier modulation for short-reach optical communications ", IEEE Photonics Technology Letters, vol. 27, no. 3, pp. 284-287, Feb. 2015.

[22] N. Eiselt, D. Muench, A. Dochhan, H. Griesser, M. Eiselt, and J. P. Elbers, "Performance comparison of 112-Gb/s DMT, Nyquist PAM4, and partial-response PAM4 for future 5G ethernet-based front haul architecture", IEEE Journal of Lightwave Technology, vol. 36, no. 10, pp. 1807-1814, May 2018.

[23] R. Linden, N. C. Tran, E. Tangdiongga, and T. Koonen, "Optimization of flexible non-uniform multilevel PAM for maximizing the aggregated capacity in PON deployments", IEEE Journal of Lightwave Technology, vol. 36, no. 12, pp. 2328-2336, Jun. 2018.

[24] R. Bai, Q. Wang, and Z. Wang, "Asymmetrically clipped absolute value optical OFDM for intensity-modulated direct-detection systems", IEEE Journal of Lightwave Technology, vol. 35, no. 17, pp. 3680-3691, Sep. 2017.

[25] M. Chen, Q. Chen, H. Zhou, Z. Zheng, J. He, and L. Chen, "Low-complexity receiver using under sampling for guard-band SSB-DDO-OFDM", IEEE Photonics Journal vol. 9, no. 4, Article no. 7203012, Aug. 2017.

[26] J. A. Altabas, S. Rommel, R. Puerta, D. Izquierdo, J. I. Garces, and I. T. Monroy, "Nonorthogonal multiple access and carrierless amplitude phase modulation for flexible multiuser provisioning in 5G mobile networks", IEEE Journal of Lightwave Technology, vol. 35, no. 24, pp. 5456-5463, Dec. 2017.

[27] C. C. Wei, K. Z. Chen, L. W. Chen, C. Y. Lin, W. J. Huang, and J. Chen, "High-capacity Carrierless amplitude and phase modulation for WDM long-reach PON featuring high loss budget", IEEE Journal of Lightwave Technology, vol. 35, no. 4, pp. 1075-1082, Feb. 2017.

[28] N. Liu, X. Chen, C. Ju, and R. Hui, "40-Gbps vestigial

sideband half-cycle Nyquist subcarrier modulation transmission experiment and its comparison with orthogonal frequency division multiplexing", Optical Engineering, vol. 53, no. 9, Article no. 096114, Sept. 2014.

[29] Z. Li, M. S. Erkılınc, K. S. Sillekens, L. Galdino, T. Xu, B. C. Thomsen, P. Bayvel, and R. I. Killey, "Spectrally efficient 168 Gb/s/λ WDM 64-QAM single-sideband Nyquist-subcarrier modulation with Kramers–Kronig direct-detection receivers", IEEE Journal of Lightwave Technology, vol. 36, no. 6, pp. 1340-1346, Mar. 2018.

[30] J. Shi, J. Zhang, N. Chi, and J. Yu, "Comparison of 100G PAM-8, CAP-64 and DFTS OFDM with a bandwidth-limited direct-detection receiver", Optics Express, vol. 25, no. 26, pp. 32254-32262, Dec. 2017.

[31] M. S. Erkılınc, S. Pachnicke, H. Griesser, B. C. Thomsen, P. Bayvel, and R. I. Killey, "Performance comparison of single-sideband direct detection Nyquist-subcarrier modulation and OFDM", IEEE Journal of Lightwave Technology, vol. 33, no. 10, pp. 2038-2046, May 2015.

[32] K. Zou, Y. Zhu, and F. Zhang, "800 Gb/s (8×100 Gb/s) Nyquist half-cycle single-sideband modulation direct-detection transmission over 320 km SSMF at C-band", IEEE Journal of Lightwave Technology, vol. 35, no. 10, pp. 1900-1905, May 2017.

[33] Z. Li, M. S. Erkılınc, K. Shi, E. Sillekens, L. Galdino, T. Xu, B. C. Thomsen, P. Bayvel, and R. I. Killey, "Digital linearization of direct-detection transceivers for spectrally efficient 100 Gb/s/λ WDM metro networking", IEEE Journal of Lightwave Technology, vol. 36, no. 1, pp. 27-36, Jan. 2018.

[34] Y. Zhu, K. Zou, and F. Zhang, "C-band 112 Gb/s Nyquist single sideband direct detection transmission over 960 km SSMF", IEEE Photonics Technology Letters , vol. 29, no. 8, pp.651-654, Apr. 2017.

[35] X. Ruan, K. Li, D. J. Thomson, C. Lacava, F. Meng, I. Demirtzioglou, P. Petropoulos, Y. Zhu, G. T. Reed, and F. Zhang, "Experimental comparison of direct detection Nyquist SSB transmission based on silicon dual-drive and IQ Mach-Zehnder modulators with electrical packaging", Optics Express, vol. 25, no. 16, pp. 19332-19342, Aug. 2017.

[36] Y. Zhu, K. Zou, Z. Chen, and F. Zhang,"224 Gb/s optical carrier-assisted Nyquist 16-QAMhalf-cycle single-sideband direct detection transmission over 160 km SSMF", IEEE Journal of Lightwave Technology, vol. 35, no. 9, pp.1557-1565, May 2017.

[37] K. Zhong, X. Hou, Y. Wang, L. Wang, J. Yuan, C. Yu, A. P. T. Lau, and C. Lu, "Experimental demonstration of 608Gbit/s short reach transmission employing half-cycle 16-QAM Nyquist-SCM signal and direct detection with 25Gbps EML", Optics Express, vol. 24, no. 22, pp. 25057-25067, Oct. 2016.

[38] L. N. Binh, "Optical modulation advanced techniques and applications in transmission systems and networks", Taylor and Francis Group, LLC, Boca Raton, London, New York, CRC Press, 2018.

[39] J. M. Senior, "Optical fiber communications principles and practice", Prentice Hall, Financial Times, England, 2009.

[40] G. P. Agrawal, "Fiber-Optic Communication Systems", Wiley-Interscience, A John Wiley, Sons, New York, 2002.

[41] M. Ghazisaeidi, L. Schmalen, P. Tran, P. Brindel, A. C. Meseguer, Q. Hu, F. Buchali, and G. Charlet, "Advanced C+L-band transoceanic transmission systems based on probabilistically shaped PDM-64-QAM", IEEE Journal of Lightwave Technology, vol. 35, no. 7, pp. 1291-1299, Apr. 2017.

[42] D. Soma, S. Beppu, Y. Wakayama, K. Igarashi, T. Tsuritani, I. Morita, and Masatoshi Suzuki, "257-Tbit/s weakly coupled 10-mode C + L-band WDM transmission", IEEE Journal of Lightwave Technology, vol. 36, no. 6, pp. 1375-1381, Mar. 2018.

[43] C. Li, F. Zhang, Y. Zhu, M. Jiang, Z. Chen, and C. Yang, "Fiber nonlinearity mitigation in single carrier 400 G and 800 G Nyquist-WDM systems", IEEE Journal of Lightwave Technology, vol. 36, no. 17, pp. 3707-3715, Sep. 2018.